Determining Emission Factors from Marine Vessels Employing Differential Optical Absorption Spectroscopy (DOAS) and Tunable Diode Laser Absorption Spectroscopy (TDLAS)

Aida Khanbabakhani

A Thesis submitted to the
Faculty of Graduate Studies
in Partial Fulfillment of the Requirements for the Degree
of Master of Science

Graduate Program
Atmospheric Chemistry, York University, Toronto, Ontario

June 2018

Abstract:

High SO_2 concentrations are harmful to human health and impact climate by affecting cloud formation. Ship contrails are the major source of SO_2 in the open-ocean and impact coastal region air quality. The International Maritime Organization (IMO) regulates SO_2 emissions by requiring ships to use fuel with varying degrees of sulfur depending distance from land. Due to lack of techniques for measuring emissions, regulations are often violated, leading to higher pollution levels. In this thesis, a method was developed to measure SO_2 emission factors and the sulfur content of fuels for individual marine vessels and trucks passing the measurement site with simultaneous remote measurements of SO_2 and CO_2 using active-DOAS and TDLAS. A demonstration of the feasibility of the project was carried out by measuring sulfur dioxide (SO_2) and carbon dioxide (CO_2) in real ship plumes along with ship schedule information at a field site near the Welland Canal, Ontario.

Table of contents

List of tables

List of Figures

1. Introduction:

1.1- Sulfur emission

The main natural sources of sulfur compounds to the atmosphere on a global scale are volcanoes, which emit large quantities of SO_2, and oceanic sources of dimethyl sulphide (DMS) from phytoplankton (Textor *et al*., 2004). However, Brasseur *et al*. (1999) have noted that most of the SO_2 emissions have anthropogenic sources. Sulfur dioxide (SO_2) is a main constituent in the tropospheric sulfur cycle. Besides the natural emissions of dimethyl sulfide (DMS), anthropogenic emissions of SO_2 are quantitatively the most important emissions in the sulfur cycle (Berglen *et al*., 2004). The major anthropogenic sources of sulfur to the atmosphere are coal and oil combustion (for generation of electricity and transport purposes), oil refining and smelting of ores, while some of the main emission sectors are: transportation, industry, international shipping, waste, residential heating and energy production. SO_2 is present in motor vehicle emissions as a result of combustion of fossil fuels that contain organic sulfur; however marine fuels currently have the highest sulfur content. SO_2 in the exhaust gas is derived completely from the fuel sulfur content as most of the sulfur is converted to SO_2 during the combustion process. Other products of combustion are: Volatile Organic Carbons (VOCs), NOx, particulate matter (PM), soot particles and secondary inorganic sulfate particles, which is the result of atmospheric oxidation of SO_2.The other byproduct of combustion to a lesser extend is SO_3, which reacts very quickly with H_2O in the exhaust to form H_2SO_4. The amount of SO_3 in the exhaust depends on the combustion temperature. Actual steady-state levels of SO_3 are normally of the order of 3% of the total sulfur in the fuel. The SO_2 will become oxidized to sulfuric acid as well but at a slower rate, either through gas phase reactions with OH or through aqueous phase oxidation mechanisms (Flagan and Seinfeld, 1988). Emitted SO_2 can be converted to H_2SO_4 as quickly as 20-30% per hour (Lack *et al*., 2009) by both homogenous and heterogeneous pathways in the atmosphere but under dry conditions it is much

slower, on the order of a few percent per hour. Moldanova *et al*. (2009) revealed that only a few percent of other sulfur species such as H_2SO_4 and sulphate particles are present in ship plume other than SO_2.

High SO_2 concentrations are harmful to human health. When breathed in, it irritates nose, throat and airways to cause coughing, shortness of breath or tight feeling around the chest (U.S. EPA, 1994). SO_2 emissions are an important environmental issue because they are a major precursor to ambient particulate matter concentrations. SO_2 reacts with air pollutants to form sulfate particles which are constituents of fine particulate matter (PM). Inhalation of particulate matter has been associated with different respiratory and cardiovascular health issues (U.S. EPA, 2008). All SO_2 concentrations results in acidic deposition that is harmful to vegetation as it increases foliar injury and decreases plant growth. H_2SO_4 can accelerate the corrosion of materials (metals, concrete and limestone) that are used in buildings and monuments (U.S. EPA, 1982). Also. high SO_2 concentrations have cooling effects through formation of cloud condensation nuclei (CCN) and results in increasing the cloud albedo and lifetime of clouds (Lohmann and Feichter, 2005).

One of the important losses of SO_2 is oxidation through OH addition in the gaseous phase under dry conditions (i.e. clear skies, no clouds, fogs or condensed water) (Stockwell and Calvert, 1983).

$$SO_2 + OH + M \rightarrow HSO_3 + M \qquad \text{(R1)}$$

$$HSO_3 + O_2 \rightarrow SO_3 + HO_2 \qquad \text{(R2)}$$

$$SO_3 + H_2O_{(g)} + M \rightarrow H_2SO_4 + M \qquad \text{(R3)}$$

SO_2 is very soluble in water. Therefore, when water (rain, clouds, fog, etc.) is present oxidation steps are different than the dry mechanism indicated above. An equilibrium forms between SO_2 in

the gas phase and SO_3^{2-} in liquid phase. The reactions involved in clouds are:

$SO_{2\,(g)} + H_2O_{\,(l)} \Leftrightarrow H_2SO_3$ (R4)

$H_2SO_3 \Leftrightarrow HSO_3^- + H^+$ (R5)

$HSO_3^- \Leftrightarrow SO_3^{2-} + H^+$ (R6)

SO_3^{2-} becomes further oxidized to SO_4^{2-} by reacting with dissolved ozone (O_3).

$SO_3^{2-} + O_{3(aq)} \rightarrow \quad SO_4^{2-} + O_{2(aq)}$ (R7)

Sulphate in the cloud or fog droplets is eventually lost to the ground through wet deposition and contributes to acid rain. H_2SO_4 has a low vapor pressure, thus it quickly nucleates to forms small particles which can act as cloud condensation nuclei (CCN) influencing cloud formation. Therefore, the clouds that are formed have more and smaller droplets whereas in normal conditions, clouds have less and larger droplets. This results in an increase in cloud albedo, which has indirect aerosol cooling effects since solar radiation is scattered back to space.

1.2-Ship emissions

Shipping plays an important role in the global transportation of goods. In 2013, 9.6 billion tons of shipping was performed with an estimated growth rate of 3.8% annually (UNCTAD, 2014). While coal use has decreased significantly in Canada and sulfur in the fuel from land-based transportation sources such as gasoline and diesel have also been decreased significantly, ship emissions of SO_2 are increasingly becoming a more significant contributor to the SO_2 emissions budget in some regions, as many regions have not yet restricted ships from using high sulfur content fuels and oceanic shipping is steadily increasing (UNCTAD, 2014). Eyring *et al*. (2005) noted that pollutant emissions from marine ships are considered to be the least regulated pollutants. Ship emissions

significantly contribute to the pollution in coastal regions since 70% of the marine emissions take place within 400 km of coastal lines (Corbett *et al*., 2000). Ship engines have been developed to be able to burn heavy fuel oils (HFO) with a very high sulfur content (0.1-4.5% by weight) that are waste products of oil refineries and thus very inexpensive (Endresen *et al*., 2005). These engines are considered to be highly efficient as they convert most of the carbon in the fuel to CO_2. However, they emit large amount of NO_x, SO_2 and particulate matter (direct and secondary PM). The European Commission, (2002) indicated that within 10 years; SO_2 emission from ships could be equivalent to all the land-based emissions along with emissions from all transport modes, plant combustion and heating engines consuming liquid fuels. Williams *et al*. (2009) compared emission factors from commercial marine vessels to those from other mobile sources: the large diesel engines in marine vessels emit more NO_X than other sources and this is also true for SO_2 emission. The US EPA (2008) currently cap sulfur in motor fuels at less than 0.005% compared to 0.5-4.5% in marine fuels. It is estimated that commercial marine vessels contribute 30% of total anthropogenic NO_X emissions and nearly 8% of total anthropogenic SO_2 on a global scale (Corbett *et al*., 2007; Eyring *et al*., 2005 and International Council on Clean Transportation, 2007).

1.3- Environmental Impacts of Shipping

Corbett *et al.* (2007) modeled the expected increase in mortality due to the increased particulate matter (PM) from ship emissions and concluded that the PM from ship emissions causes 60,000 cardiopulmonary and lung cancer deaths each year, with the majority of deaths in coastal areas in Europe, East Asia and South Asia. In plants, particulate matter can clog stomatal openings and interfere with photosynthesis functions. Matthias *et al*., 2010 reported that SO_2 emissions by ships lead to an enhanced sulfate concentration of 10-50% in coastal areas that increase the acidification process by acid rain. Jonson *et al*. (2000) performed emission modeling and indicated that ship

transportation has a noticeable contribution to acid rain in many parts of Europe. The “critical load of acidity” is used to measure the effect of acidity, defined as the maximum deposition of sulfur and nitrogen not causing harmful leaching of acidity.

1.4- Ship emission regulations

International Maritime Organization (IMO) is an agency of the United Nations that adopted Marine pollution, MARPOL Annex VI in 1997 (MARPOL is International Convention for the Prevention of Pollution from Ships) (The Magazine of the United Nations, May 2017). The MARPOL Annex VI regulated the amount of sulfur in ship fuels with the goal of reducing SO_2 emissions in populated coastal areas. This annex includes a global cap of 4.5% on sulfur content in marine fuels and contains provisions allowing for special SO_x Emission Control Areas (SECA) that is established with more strict limits on sulfur emissions. In these areas, the sulfur content of fuel oil used on board must not exceed 1.5% by mass. Alternatively, ships must install an exhaust gas cleaning system (scrubbers) or use any other technological method to limit SO_x emissions. The Baltic Sea Area, the North Sea and English Channel were designated as SECA in the Protocol, starting at the end of 2007. In 2010 the maximum SECA sulfur level was decreased to 1% and then it was further reduced to 0.1% in 2015. This is illustrated in Figure 1 were both the global cap and SECA limits of sulfur content are plotted. In recent years, Canada and the U.S. worked with the International Maritime Organization to designate an Emission Control Area in North American coastal waters. The emission control area establishes a 200-nautical-mile zone around North American coastlines and imposes stricter standards on emissions from large ships including oil tankers, cargo ships and cruise ships when they are operating in this zone. The Emission Control Area came into effect on August 1, 2012 requiring that fuel used by the vessels be below 1.0% sulfur. Beginning in 2015, fuel used by vessels operating in these areas cannot exceed 0.1% sulfur.

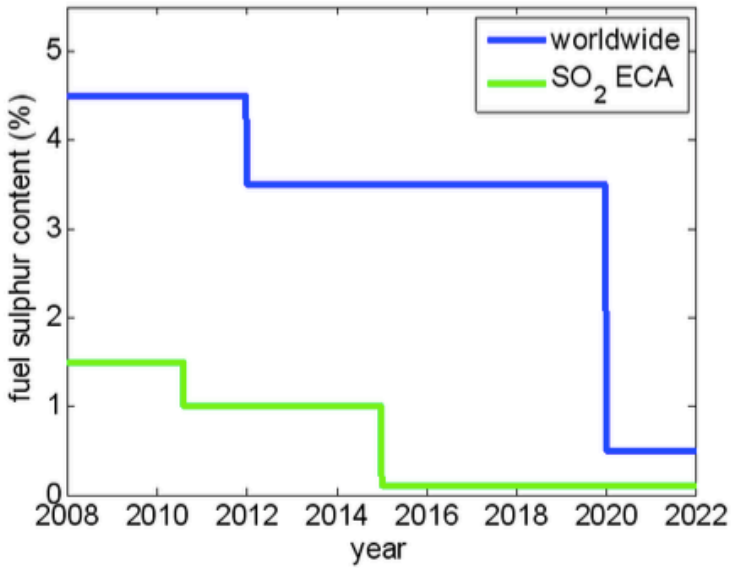

Figure 1: Fuel sulfur content (%) for worldwide and SECA areas. The limit is decreasing. The worldwide limit in 2020 will be 0.5% and 0.1% in SECA areas (Berg *et al*., 2010).

There is a significant price difference between low and high sulfur fuel oil and the price for low sulfur fuel oil will further increase due to a rising demand. The major cost of shipping depends on the cost of fuel and therefore there is an economic incentive to run ships with cheaper fuel oil such as residual fuel containing high sulfur. Companies that violate rules regarding fuel sulfur content have higher economic advantages. Therefore, there is a question of whether the new regulations are being respected or not since efficient surveillance methods for ship emissions are missing and ships are capable of carrying different fuel types in separate tanks. Also, ocean going ships usually switch from high to low sulfur fuel upon arriving in Sulfur Emission Control Areas (SECA). Authorities usually perform inspections by entering ships onboard at the harbors and analyzing fuel samples. This technique is expensive and time consuming. Moreover, only few inspections are conducted at specific time intervals and not all ships are being inspected. What is more important is that there is no efficient technique for controlling ships in international waters where they must run with specific fuel. Berg *et al*. (2010) mentioned that a method needs to be implemented for emission controls of marine vessels similar to speed cameras used for vehicles.

1.5-Previous studies on emission measurements

Recently, there have been different techniques proposed for in-use emission measurements such as close observation of ship emissions where an air quality measurement system was implemented with close observation of ship emissions in order to determine the compliance of MARPOL VI policy regarding sulfur content of ship fuels in SECA (Kattner *et al.,* 2015). The sulfur content of each ship passing by the measurement site was calculated using long path SO_2 and CO_2 measurements along with ship position data. Kattner *et al.,* (2015) used an automatic identification system (AIS) receiver that identified passing ships. AIS is a system designed in order to avoid collision among ships and it broadcasts ship information such as position, identification and speed. They measured the increase of SO_2 and CO_2 caused by the ship emission and the ratio of SO_2 and CO_2 peaks (concentration) was used in order to determine the sulfur content of the ship fuel.

Another method is using an open-path Remote Sensing Device to measure marine vessels emissions as described by Burgard and Bria (2016). This study is considered to be the first use of an open-path Remote Sensing Device (RSD) that measured marine vessels emissions. This method measured NO_X and SO_2 emission from 16 distinct ships while they passed under the Lion Gate Bridge in Vancouver, B. C. As a ship passed under the bridge, the ship plume emitted from the stack would passively intersect the RSD beam on top of the bridge. Emissions from ships were measured noninvasively by the Fuel Efficiency Automobile Test (FEAT) RSD developed at the University of Denver. This instrument had a light source that sent a UV/IR beam in to a detector separated by an open path (path length = 24 meters) while the plume was passively being transported to the instrument.

The other method is remotely flying on airplane nearby ships (Beecken *et al*., 2014 and Lack *et al*., 2011). Beecken *et al*., (2014) performed airborne ship emission measurements for SO_2 and CO_2

gases from different ships at open sea in order to obtain emission factors. A flight-modified Picarro G230-m and modified Thermo 43i-TLE trace gas monitor were used for CO_2 and SO_2 measurements, respectively. The measurement mode was modified in order to obtain as many measurements as possible during the short time in which the aircraft traverses a plume before it dilutes. Lack *et al*., (2011) also studied atmospheric emission of gas and particulate matter from a large ocean-going vessel. The vessel switched from high sulfur to low sulfur fuel prior to arrival at the regulated coastal waters of California. In that study, the NOAA research aircraft intercepted the Margrethe Maersk (MM) marine vessel. Initially MM was running on HFO containing 3.15% sulfur and then gradually switched to Marine Gas Oil (MGO) containing 0.07% sulfur. The emission factor for SO_2, SO_4 and CCN dropped by 91%, 97% and 97.5%, respectively as the fuel was switched to low sulfur. Also, compliance with the fuel sulfur limit resulted in noticeable reduction of 91% in EF(SO_2).

In a study by Cappa *et al*., (2014), emission factors for PM and trace gases (CO, SO_2, HCHO and NO_x) were measured using the plume intercept method which is known as the "sniffer method". The concentrations of the pollutants were measured in a plume that was intercepted downwind of a marine vessel, the NOAA ship Miller Freeman that operated a medium speed diesel engine on low sulfur marine gas oil (~ 0.1% sulfur content by weight). Particle phase instrumentation included a high-resolution time of flight aerosol mass spectrometer. This study showed that there was no relationship between the SO_2 emission factor (EF) and vessel speed. EF(SO_2) does not primarily depend on engine load as the emission factor strongly depends on the fuel sulfur content. The obtained EF(SO_2) values confirmed that Miller Freeman vessel was running on low sulfur fuel which was estimated to be 0.097 ± 0.011% sulfur by weight. Also, the emission factor for particulate SO_4^{2-} were negligible suggesting that the SO_3 emissions were very small.

In a study by Williams *et al*., (2009), samples of passing plumes were taken into a portable emission measuring equipment. Emission factors from different types of ships under different operating conditions (underway and stationary) were determined during the Texas Air Quality Study of 2006 in the Houston Ship Channel and the Gulf of Mexico on board the NOAA research vessel Ronald H. Brown (RHB). Non-dispersive infrared instrument (Li-Cor Model LI-7000) and pulsed UV-fluorescence (Thermo Electron Corp. Model 43s) were used for CO_2 and SO_2 measurements, respectively.

McLaren *et al*., (2012) performed stationary measurements in environments affected by ship activities. The use of Differential Optical Absorption Spectroscopy (DOAS) was demonstrated for passive detection of NO_2 and SO_2 in ship plumes on the west coast of Canada in 2005. Although CO_2 was not measured, the NO_x/SO_2 ratios in the plumes were compared to those in local inventories, as a way for surveying the emissions of SO_2 from many ships in a pre-SECA era. The median NO_2/SO_2 molar ratio from 17 different ship plumes were similar to the NO_x/SO_x emission ratio for marine vessel emissions in a 2005 inventory.

1.6-Emission Factors (EF)

An emission factor (EF) represents the amount of pollutant produced per unit amount of activity associated with the release of the pollutant (e.g., VOC emitted per km driven). EFs are important since they are used to calculate the total emission from a source when used as input in emission inventories, which are typically used in Air Quality Management Plans and emission inventory modeling. Emission inventories are often used in order to study pollution sources and to evaluate the relative significance of them. It is possible to measure fuel-based emission factors (i.e., amount of pollutant emitted per amount of fuel burned) from sources by measuring both the pollutant and a surrogate for fuel burned (CO_2) in the source plume, assuming that the majority of the carbon in

the fuel is emitted as CO_2 after combustion. In reality, minor amounts of the carbon are emitted as carbon monoxide (CO), VOCs and particulate carbon (elemental carbon and organic carbon in particles). Also, sulfur content in the fuel is converted almost completely to SO_2 in the exhaust gas. Combustion of fuel in marine vessels is usually complete and most of the sulfur emitted is in the form of SO_2. Therefore, SO_2 can be used as a proxy for the sulfur content in the emission plumes.

Williams *et al*., (2009) calculated emission factor using two assumptions: 1. that all of the carbon in the fuel is converted to CO_2 and 2. that the average mass fraction of the carbon in the fuel is 0.865 (around 87%) (Cooper, 2003). Beecken *et al*., (2014) used the following formula to calculate the amount of sulfur in a fuel and also to calculate the emission factor of SO_2 while making similar assumptions as William *et al*., (2009):

$$EF\ \mathrm{SO2}\left(\frac{g\ SO2}{Kg\ Fuel}\right) = \frac{\Delta xSO2}{\Delta xCO2} \times \frac{M\ S02}{M\ C} \times Wc\ \times 10^3 (g.kg^{-1}) \qquad \text{Equation 1}$$

where ΔX_{SO2} and ΔX_{CO2} are the enhanced mixing ratios of SO_2 and CO_2 measured in the plume (background subtracted), M_{SO2} and M_C are the molecular weights of SO_2 and C respectively and Wc is the fractional composition of carbon in the fuel. The percentage of sulfur in the fuel is given by:

$$\%S\ = \frac{\Delta x\ (SO2)}{\Delta X\ (C02)} \times \frac{M\ (S)}{M\ (C)} \times\ Wc\ \times 100\% \qquad \text{Equation 2}$$

where M(S) and M(C) are the atomic weights of Sulfur and carbon, and other parameters are as previously defined.

1.7-Tunabale Diode Laser Absorption Spectroscopy (TDLAS) Theory

Open Path Tunable Diode Laser Absorption Spectroscopy (TDLAS) is used in atmospheric pollutant studies. TDLAS focuses on a single absorption feature in the near infrared region that is specific to the desired species. It exploits the unique light absorption characteristic features of gases for laser-based trace gas detection. It is a very strong tool for highly selective and sensitive measurements with robust technologies for monitoring of trace gases. It measures the attenuation of light due to absorption of a diode laser beam at a certain wavelength that travels through a measurement path. Since each molecule absorbs light at a specific wavelength, a certain diode laser is needed for the measurement of different gases. A TDL spectrometer requires a reference cell with known concentration of the target molecule that has absorbances in the spectral range of interest. The sealed reference cell provides an absorption signal that enables the line locking for the diode laser. Also, the reference cell is needed during the initial search for suitable lines with no atmospheric interferences. The wavelength of laser is scanned over a small range that contains the absorption line of the trace gas; however, the absorption line also contains regions with no absorptions (baseline). A photo-detector measures the transmitted light intensities. The baseline region shows the attenuation of light due to effects other than absorption of the molecule of interest such as existence of ash, dirt and dusts. There are other effects such as turbulence that cause the fluctuation of the baseline. However, the ratio of the size of the absorption feature to the baseline remains the same and represents the concentration. Signal averaging increases the signal to noise ratio. Also, modulation techniques are applied in order to achieve more noise suppression. For modulation spectroscopy, the laser injection current is modulated while the laser wavelength is tuned over the specific absorption line to accumulate the signal from the lock-in amplifier with a digital signal averager (Werle P.W. 2004). The transmitted light intensity measured by the detector is described by the Beer-Lambert law (Plane and Smith, 1995):

$$I(\nu) = I_0(\nu)e^{-N\sigma(\upsilon)L} \qquad \text{Equation 3}$$

Where σ(ν) is the frequency dependent absorption cross section (m^2), L is the path length (m) and N is the number density of the absorbing species ($\frac{molecule}{m^3}$).

TDLAS has been used several times to measure different atmospheric trace gases such as H_2O_2, HCHO at sub-ppbv detection limits (Mackay *et al*., 1996; Harris *et al.,* 1992; Harris *et al.,* 1989; Schiff *et al.,* 1983; Schiller *et al*., 2001). In a study by Schiller *et al*., (2001) ambient gas phase nitrous acid (HONO) was measured by TDLAS. Also, a 1.5 m white cell having a folded path length of 126 m and total volume of 27 liters was used. TDLAS directly sampled HONO in the gas phase minimizing the possibility of the formation of artifacts with higher sensitivity. A 10 slm flow was introduced through the cell at a reduced pressure of 30 torr that resulted in the residence time of around 6 seconds within the cell. Ambient and background spectra were averaged to 30 minutes sampling interval and the average minimum detectable concentration of HONO was measured to be 300 pptv.

1.8- Differential Optical Absorption Spectroscopy (active-DOAS) Theory

Differential optical absorption spectroscopy (DOAS) is a spectroscopic technique that identifies a wide variety of gases by analyzing a spectral ranges of wavelengths of light absorbed by each gas (Platt *et al*., 1979). The advantage of DOAS is that, it is a powerful remote sensing technique that enables direct and sensitive detection for multiple trace gases simultaneously without influencing their chemistry. It uses specific narrow band absorption structures of the different trace gases for detecting and estimating their concentrations by separating them from the broadband features caused by factors including atmospheric scattering (Raleigh and Mie) and broad band absorption.

Currently, there are two modes for DOAS application based on the origin of the collected light: a passive mode called MAX-DOAS and an active mode known as active-DOAS. A natural light source such as the moon or the sun is used in passive-DOAS techniques collecting either direct or scattered light from the source. On the other hand, active-DOAS utilizes an artificial light source such as high pressure Xe-arc lamps or light emitting diodes. This technique utilizes a telescope generating collimated light beam through a well-defined path-length in the open atmosphere. In MAX-DOAS (Honninger, 2004), sky

scattered sunlight is used to measure information that can be related to the vertical distribution of absorbers in the atmosphere. Platt *et al*., 1979 used an artificial light source, taking simultaneous measurements of atmospheric CH_2O, O_3 and NO_2. DOAS was the first technique that directly measured radical species such as OH (Perner *et al*., 1976), NO_3 (Platt *et al*., 1980a), OClO, BrO (Sanders *et al*., 1989), IO (Alicke *et al*, 1999) in the atmosphere and glyoxal (Volkamer, 2005) in the atmosphere.

Long path DOAS is considered to be the basic active-DOAS technique in which a telescope generates collimated light from a light source that is reflected by a retro-reflector at a distance and returning the light over the open path to the telescope where it is received and directed to the spectrometer using a fiber optic.

The DOAS principle is based on Beer-Lambert's law (Plane and Smith, 1995):

$$I(\lambda) = I_0(\lambda)e^{-\sigma(\lambda)Ln_i} \qquad \text{Equation 4}$$

where $I_0(\lambda)$ is the initial light intensity and $I(\lambda)$ is the transmitted intensity of the light of wavelength λ after passing through an air sample of length L (cm) with concentration of analyte n_i $(\frac{molecule}{cm^3})$ and

absorption cross-section σ (λ). The optical density (D) is defined as:

$$D = \ln\left[\frac{I_0\lambda}{I\,\lambda}\right] = \sigma(\lambda)L\,c \qquad \text{Equation 5}$$

The concentration of the gas species is calculated by rearranging the above equation:

$$c = \ln\left[\frac{I_0\lambda}{I\lambda}\right]\frac{1}{\sigma\,(\lambda)L} = \frac{D}{\sigma\,(\lambda)\,L} \qquad \text{Equation 6}$$

However, the equation above needs to be extended, as it is important to account for the Rayleigh and Mie scattering of light in the atmosphere. Rayleigh scattering is the scattering of photons by air molecules as light traverses through an air parcel and is inversely proportional to the fourth power of the wavelength. Mie scattering is the scattering of light by aerosol particles that are having the same dimensions as the wavelength of the incident light. It depends on wavelength as the index of refraction of particle depends on wavelength.

Now the atmospheric absorption from a single absorbing trace gas can be expressed by accounting for both Rayleigh and Mie scattering:

$$I(\lambda) = I0\,(\lambda)e^{L(-\sigma(\lambda)c\,+\,\varepsilon R(\lambda)\,+\,\varepsilon M\,(\lambda))} \qquad \text{Equation 7}$$

Where $\varepsilon^R(\lambda)$ is the Rayleigh extinction coefficient and is equal to $\sigma^R(\lambda)$. n_{air} (the first is the cross section of the Rayleigh scattering and the second is the concentration of air) and $\varepsilon^M(\lambda)$ is the Mie extinction coefficients and is equal to $\sigma^M(\lambda)$. n_{air} (where the first is the cross section of the Mie scattering).

However, it is important to account for the absorption of various trace gases present in the atmosphere that absorb within the same wavelength interval. Therefore, the equation above is extended as below:

$$I(\lambda) = I0(\lambda)e^{-\mathrm{L}(\ (\Sigma\sigma_{\mathrm{i}}(\lambda).\mathrm{c_i}) + \varepsilon_{\mathrm{R}}(\lambda) + \varepsilon_{\mathrm{M}}\ (\lambda))} \qquad \text{Equation 8}$$

where i denotes for the i^{th} absorbing species.

Determining the true intensity of light transmitted in the absence of absorbers is difficult. Therefore, "differential absorption" which is the component of the total absorption of any molecule that quickly varies with wavelength is measured (Platt and Stutz, 2008). The absorption cross-section of a trace gas is separated into two components of broadband and narrowband:

$$\sigma_{\mathrm{i}}(\lambda) = \sigma_{\mathrm{i,o}}(\lambda) + \sigma_{\mathrm{i}}^{'}(\lambda) \qquad \text{Equation 9}$$

where $\sigma_{\mathrm{i,o}}(\lambda)$ is the broadband component varying slowly with the wavelength while $\sigma_{\mathrm{i}}^{'}(\lambda)$ is the narrowband component that varies rapidly with wavelength.

Beer-Lambert's law is modified combining the narrow and broadband components in Equation 10 below:

$$I(\lambda) = Io(\lambda)e^{-L(\Sigma\sigma_{\mathrm{i}}{}'(\lambda)\ \mathrm{c_i})}e^{-\mathrm{L}\ (\Sigma\ \sigma_{\mathrm{io}}(\lambda)\mathrm{c_i} + \varepsilon_{\mathrm{R}}(\lambda) + \varepsilon_{\mathrm{M}}\ (\lambda))}A(\lambda)$$

where A (λ) is the attenuation factor that describes the broadband wavelength dependent transmission of the optical system.

Now, $\sigma^{'}(\lambda)$ that is the corresponding differential absorption cross-section is substituted for σ (λ) and a differential optical density, $D^{'}$ is defined as:

$$\mathrm{D}' = \ln\frac{\mathrm{I}'0(\lambda)}{\mathrm{I}(\lambda)} = \mathrm{L}\Sigma[\sigma_i'(\lambda)c_i] \qquad \text{Equation 11}$$

Thus, the concentration of absorbent i is calculated as:

$$c_i = \frac{D'}{\sigma_i'(\lambda)L} \qquad \text{Equation 12}$$

The concentration of the species of interest is directly calculated by measuring I (λ) and then solving the equation above. Finally, concentration of the trace gas is calculated by performing a least square fit of the structured absorption and providing a suitable differential absorption cross-section reference spectra for the analyzed species. The non-invasive nature of this technique enables the measurement of highly reactive radical species. A DOAS system does not require any calibrations since an accurate absorption cross-section of the trace gases is the calibration factor. The absorption cross-sections of frequently measured atmospheric trace gases by DOAS are shown in Figure 2.

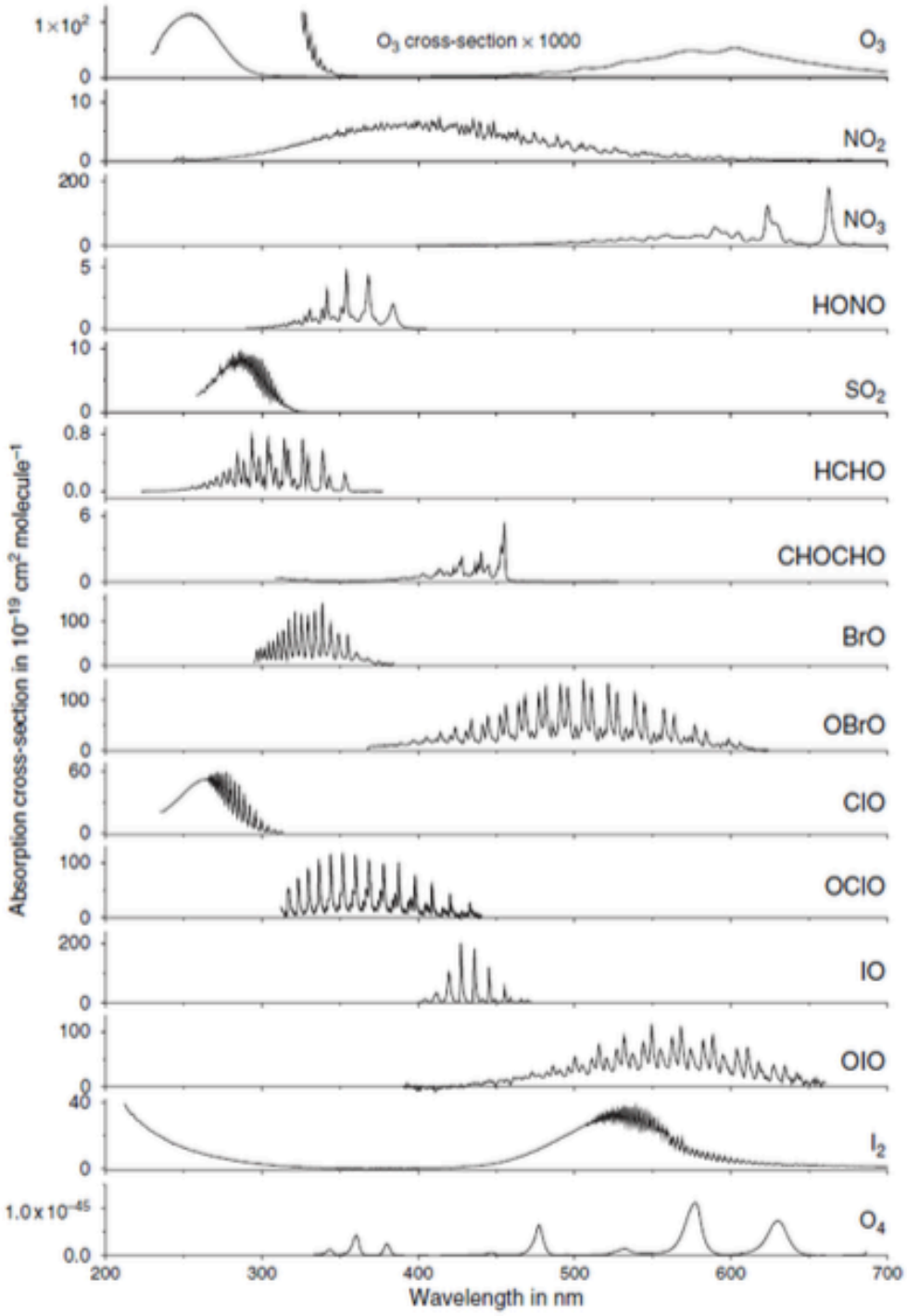

Figure 2: Absorption cross-section structures of different atmospheric trace gases measured by DOAS within the wavelength range of 200-700 (nm) (Platt and Stutz, 2008).

1.9- Purpose

This research was focused on developing a long path technique for determining emission factors (EF) of SO_2 from ships using a combination of two different spectroscopic instruments: tunable diode laser spectroscopy (TDLAS) to measure CO_2 and Differential Optical Absorption Spectroscopy (DOAS) to measure SO_2 within the same light path. In this thesis, analytical feasibility of this method is demonstrated. A short demonstration study near the Welland canal to measure real ship plumes was also completed. The field measurements serve as a feasibility test of the suitability of the combined active-DOAS/TDLAS method to remotely monitor ship emissions and sulfur content of fuel.

2- Experimental:

2.1- Work summary

During the first year of master's program, utilization of the active-DOAS instrument, measuring SO_2 mixing ratios and performing spectral fittings using DOASIS software were practiced. Also, a newly purchased TDLAS instrument was characterized. Then, for the second year of master's program, feasibility of using a combination of TDLAS and active-DOAS instruments for CO_2 and SO_2 measurements, respectively was demonstrated. First, analytical measurements were performed in laboratory in order to ensure that detecting a ship plume is possible with the use of our set-up and instruments since there is a typically very low ambient SO_2 concentration at York University (<0.5 ppb), which have fallen significantly over the last decade or two. Several active-DOAS measurements using a 10 (ppm-m) SO_2 sample cell along with a low-pass quartz filter (cut-off at 400 nm) was performed in order to simulate a high SO_2 plume and find the detection and quantification limits (3σ and 10σ) as a function of collection time. The results are presented in section 2.2. The TDLAS instrument was used to measure the CO_2 mixing ratio at a return path length of 498 m using a 30-cube aluminum retro-reflector. Measurements were taken with different

dwell times (0.1, 0.5, 1.0, 2.0, 5.0 and 10.0 sec) in order to study the noise of the instrument and determine the detection limit for CO_2 measurement. The results are presented in section 2.2.1.A pseudo calibration factor was determined for TDLAS by having an intercomparing study with a picarro instrument from Environment Canada (Section 2.2.1.1).

Initially, the plan was to use the two open path techniques simultaneously while utilizing one retro-reflector (30-Cube UV-enhanced) where the beam would transect the pollution plume of a ship. However, the return signal from the TDLAS instrument using the 30-cube UV-enhanced aluminum retro-reflector was very weak. This retro-reflector is ideally suited for UV-applications with the wavelength range of 225-700 nm and TDLAS measurements of CO_2 make absorption measurement at 1581 nm. As a result of the substandard performance of the Al retro-reflector in the near IR, a 23-element gold retro-reflector array (Unisearch Associates Inc) was purchased. The gold retro-reflector is not optimum for reflecting UV-light in the wavelength range necessary for SO_2 measurements (λ=300-320 nm). Thus, the plan for future experiments was modified to utilize two retro-reflectors side by side instead of one. This did not greatly impact the results since the two retro-reflectors were located very close to each other (within 1 m).

After ensuring that we were able to measure SO_2 and CO_2 at the temporal resolution necessary to capture a transient plume, a demonstration experiment was undertaken in the vicinity of a busy ship channel of the Welland Canal, Ontario. A simultaneous SO_2 and CO_2 detection scheme was adopted by utilizing both DOAS and TDLAS instruments with the transmitter telescopes side by side and the two retro-reflectors side by side such that both the IR and UV beams had the same path length and transected the same air mass (Section 2.3-Field experiment). The emission factor of SO_2 was calculated for marine vessels using the measured concentrations of SO_2 and CO_2 from ship plumes. The results are presented in section 3-Field work results and discussions.

2.2-Anaytical work

2.2.1- Analytical Development: TDLAS measurements of CO_2

For this project, a Unisearch RP130 Portable LasIR Near infrared TDLAS analyzer (Figure 3) was used. LasIR has a sealed CO_2 reference cell having known amounts of CO_2 gas measured with 85% peak absorption at 1581 nm. Reference cell enables the ability to line-lock the laser and to verify the instrument calibration. The laser contained in this analyzer is tuned to the frequency of the spectral feature of the selected gas by varying the laser temperature and current. The absorption feature is scanned repeatedly by fast automated changes to the current applied to the laser which rapidly changes the wavelength. Measurements of CO_2 made absorption measurement at 1581 nm using a dedicated CO_2 laser. Carbon dioxide (CO_2) was measured in an open path optical configuration. The analyzer was located on a tripod and the retro-reflector was at the opposite side of the measurement path. For this purpose, a 23-element gold retro-reflector array (Unisearch Associate Inc) was purchased. The analyzer is aligned with the retro-reflector using a riflescope attached to the telescope head. A power bar displayed at the Normal Run-time display screen indicates the return signal beam strength, which is maximized during alignment via adjustment of the X-Y-R stage. Light was sent across an open path and reflected off the retro-reflector and sent back to the analyzer. The returning beam is focused onto a detector with an off axis parabolic mirror and the photovoltaic output of the detector is sent to the LasIR analyzer via a fiber optic cable. The parameters that needed modification were the path length and dwell time. The path length entered was the total path, which is twice the separation between the analyzer and the retro-reflector. Also, dwell time can be chosen, which is the length of the time that the laser spends on scanning the absorption feature of CO_2 for a single measurement. The application software that controlled the LasIR analyzer was LasIRVeiw. It allows the transfer of data from the analyzer to a personal computer.

Different dwell times were used in order to investigate the noise characteristics of the instrument. The TDLAS measured CO_2 in ambient air with a return path-length of 498 m using the 23-element gold retro-reflector array that was located on top of the Psychology building, while the telescope was located in a laboratory on top of the Petrie Science and Engineering building (Figure 4). CO_2 mixing ratios were measured at different dwell times (0.1, 0.5, 1.0, 2.0, 5.0 and 10.0 sec) each for about 10 minutes during the afternoon of 17th February 2017. Figure 5 shows the CO_2 mixing ratio versus time in which the dwell times for each time interval are labelled. Figure 6 shows the standard deviation of the CO_2 mixing ratio as a function of the inverse of the square root of the dwell times. As might be expected, the standard deviation, which represents the noise of the instrument, is proportional to 1/√Dwell time. This indicates that the instrumental noise is random. As can be observed from Figure 6, the standard deviation decreases as the dwell time increases. The 10.0 sec dwell time has the lowest noise among the different dwell times analyzed. In order to compare the instrumental noise with different dwell times, average CO_2 concentration, standard deviation and 1/√Dwell time were calculated for each set of binned data and summarized in Table 1. To see if post processing of data is possible, the data points were binned and averaged in groups of 10 seconds (Note that 10 seconds might be an acceptable averaging time for proper measurement of a plume transient that lasts 3 minutes. This would allow 20 measurement points per 3-minute transient). For example, the points from 0.1 sec dwell time were binned/averaged in groups of 100 points, the points from 0.5 sec dwell time were binned/averaged in groups of 20 points and so on. Figure 7 represents the CO_2 concentration versus time graph for data points that are averaged to 10 seconds. The dwell times for each time interval are labelled.

As can be seen in Table 1, the data collected at different dwell times but averaged to a constant averaging period (10 sec) have noise (precision) that is not different from one another. Therefore, post averaging of data collected at short dwell times is possible (and desirable) without the loss of

precision in cases where the length of the transient plumes is not predictable in advance. Short dwell times are desirable in order to ensure that the temporal transient of a short duration plume is captured, and to observe an increase in CO_2 concentration before the plume diffuses.

Table 1 shows the detection limits (3σ) and quantification limits (6σ) for CO_2 measurements at different dwell times. The quantification limit at 0.1 s and 10.0 s dwell times are 37.44 and 25.54 ppm, respectively. These values are the lowest possible mixing ratios that TDLAS could measure for CO_2 at these dwell times. Previous ΔCO_2 values measured by other studies were investigated from several literatures in order to determine whether detecting a real ship plume is feasible with the TDLAS instrument. Williams *et al*., (2009) measured 34 ppm increase in CO_2 in a 3-minute plume coming from a tanker ship in the Gulf of Mexico in August 2009 where the air was drawn from a sampling manifold in to a non-dispersive IR instrument. In another study by Johansson *et al.*, (2011), 40 ppm of ΔCO_2 was measured by a non-dispersive IR instrument through extractive sampling by the passive exhaust plume coming from a cargo ship that took ~2 minutes. These values obtained from literature are higher than the detection limit and similar to the quantification limit determined for TDLAS. Therefore, it is concluded that detecting increases in CO_2 due to ship plumes in a marine area is feasible.

Figure 3: A Unisearch RP130 Portable LasIR Near infrared TDLAS analyzer and the CO_2 reference cell.

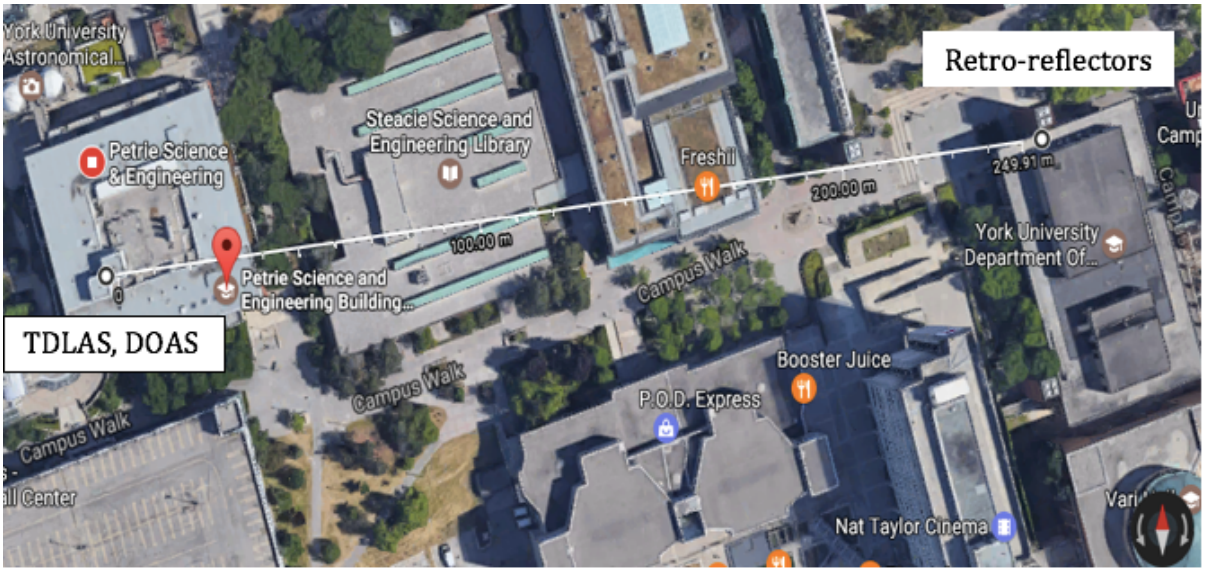

Figure 4: TDLAS and active-DOAS were located on top of the Petrie Science and Engineering building with the retro-reflectors located on top of the Psychology building.

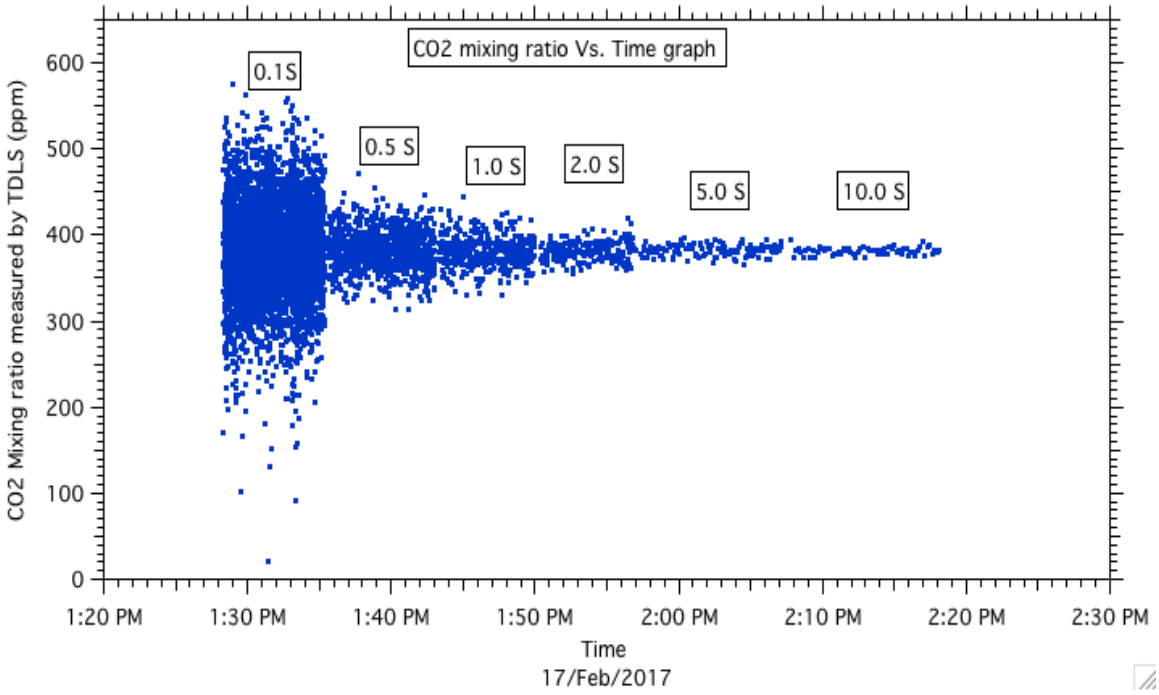

Figure 5: CO_2 mixing ratios measured at different dwell times. Dwell times are labelled on top of data points.

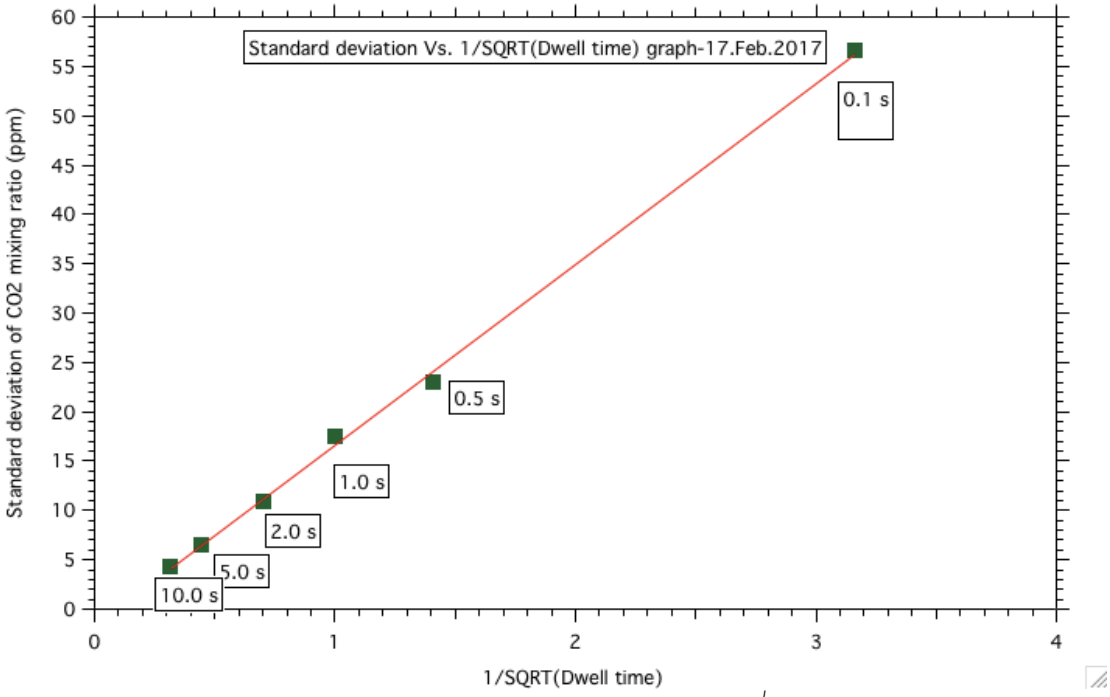

Figure 6: Noise associated with each dwell time versus 1/√Dwell time.

Table 1: The noise associated with the data points that collected at different dwell times and averaged to 10 seconds.

Dwell time (S)	Average CO_2 Concentration (ppm)	Standard Deviation of averaged data (ppm)	Detection Limit 3σ (ppm)	Quantification Limit 6σ (ppm)	Number of points averaged
0.1	382.33	6.24	18.72	37.44	100
0.5	382.55	4.05	12.16	24.31	20
1	381.26	5.19	15.56	31.13	10
2	381.25	5.21	15.64	31.27	5
5	382.30	4.80	14.39	28.79	2
10	381.44	4.26	12.77	25.54	1

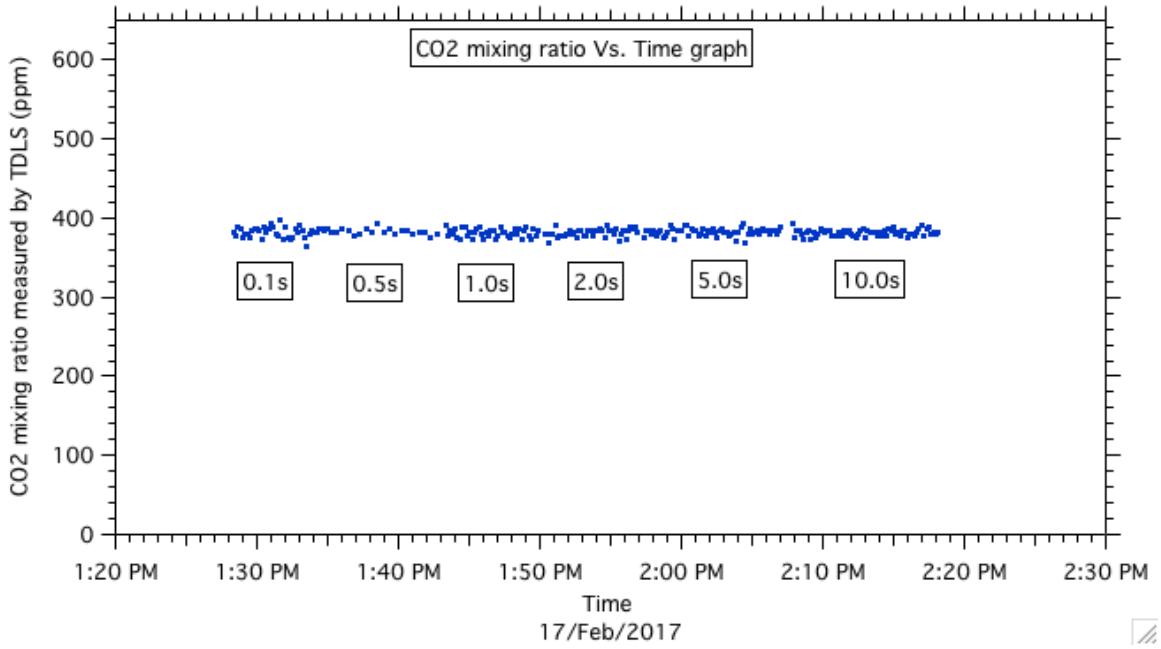

Figure 7: CO_2 mixing ratios for data points averaged to 10.0 sec. The dwell times are labelled under each group of data points.

2.2.1.1- Determining TDLAS Calibration Factor

In this section, a pseudo calibration factor is determined in order to correct CO_2 values measured by TDLAS and ensure that the TDLAS measures true values of CO_2. As a result, Picarro, which measures true values of CO_2, was selected for this purpose. The pseudo calibration factor (P) can be determined as follows:

$$P = \frac{[CO2]Picarro}{[CO2]TDLAS}$$

A Cavity Ring-Down Spectroscopy instrument (CRDS) by Picarro G2401-m (borrowed from Environment Canada) was available for this study. In CRDS, the beam from a variable-frequency laser diode enters a cavity defined by two or more high reflectivity mirrors. Picarro analyzers use a three-mirror cavity to support a continuous traveling light wave. This provides superior signal to noise compared to a two-mirror cavity that supports a standing wave. When the laser is on, the cavity quickly fills with circulating laser light. A fast photo-detector senses the small amount of

light leaking through one of the mirrors to produce a signal that is directly proportional to the intensity in the cavity. The Picarro measures CH_4 (dry and wet), CO, CO_2 (dry and wet) and H_2O. Both TDLAS and Picarro instruments were left running together on 12 May 2017 on top of the Petrie Science and Engineering building at York University for 2.5 hours. The inlet tube for the Picarro was placed outside the lab through a window for sampling with 2.0 sec synchronous time. The TDLAS instrument measured CO_2 gas with a return path-length of 498 m and 2.0 sec dwell time using the 23-element gold retro-reflector array that was located on top of the Psychology building. Figure 8 indicates the time series of CO_2 mixing ratios vs. time from both instruments. The average values of CO_2 mixing ratios measured by both instruments were used on order to calculate the pseudo calibration factor. A calibration factor of 1.008 was obtained.

The new calibration factor (P) could either be added to the software or be applied post measurement:

$$[\mathrm{CO2}]\text{True value} = \mathrm{P} \times [\mathrm{CO2}]\text{Measured}$$

For this project, the calibration factor was applied post measurement, after obtaining the emission factors.

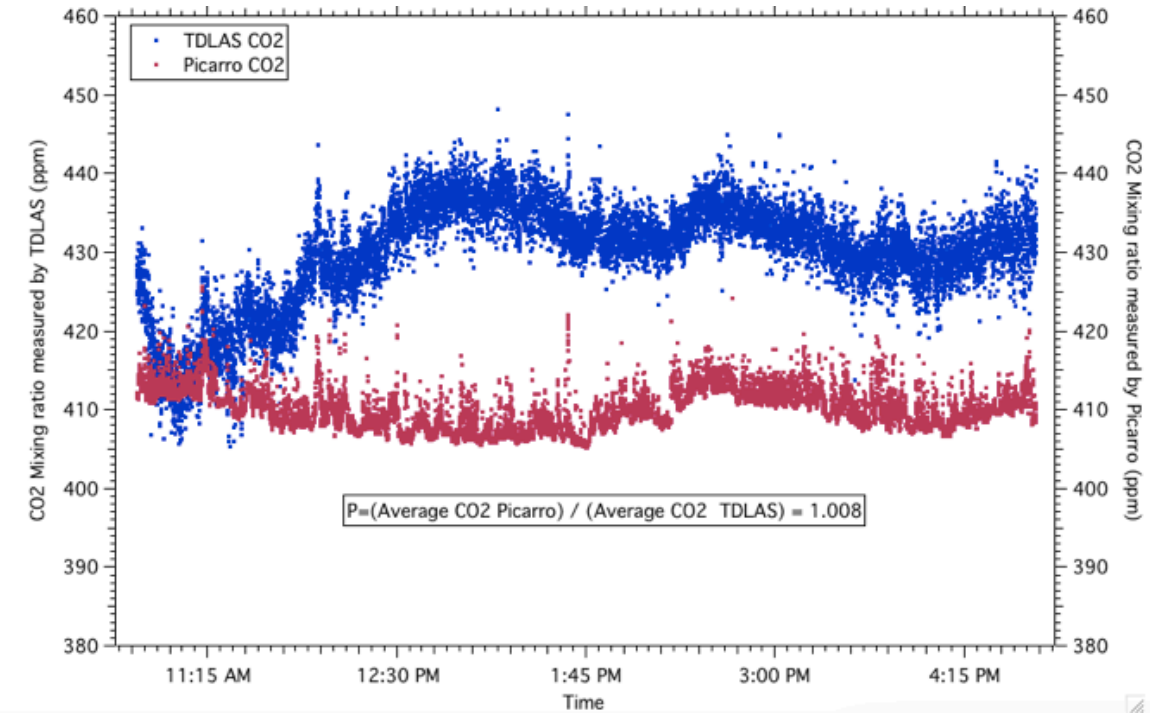

Figure 8: Time series of CO_2 mixing ratios vs. time from both TDLAS and picarro on 12 May 2017. The calculated calibration factor for TDLAS is 1.008.

2.2.2- Analytical development: Active-DOAS measurements of SO_2

The DOAS technique exploits the unique spectral absorption of SO_2 to retrieve their mixing ratios in the atmosphere. This was accomplished by coupling the light of an artificial light source; where a xenon arc lamp in the telescope sends the beam through the atmosphere to a 30-cube UV-enhanced aluminum retro-reflector (PLX, AR-30-5). The retro-reflector sends the beam back to the telescope where it is measured by a spectrometer. By knowing the spectrum of the lamp, spectral analysis of the reflected light yields absorption features of SO_2 and therefore averaged mixing ratios along the measurement path. By using the artificial light source that provides high intensities in the UV, SO_2 can be measured with high precision and time resolution.

2.2.2.1- Hardware and Spectroscopy

The active-DOAS system consisted of a modified DOAS 2000 Instrument (TEI Inc.). As presented in Figure 9, the system was composed of a coaxial Cassegrain telescope with transmitting and receiving optics combined within the instrument. A 150 W high-pressure xenon-arc lamp was employed as the light source and is placed in the focal plane of the 8" primary telescope mirror. The return light beam is focused onto a fiber optic cable 600µm diameter) by the inner portion of the primary mirror, transmitting the light into a spectrometer, a device that separates the wavelength components of light and was optimized for the species of interest. Measurement of SO_2 was performed in the UV region of the electromagnetic spectrum by a USB2000 spectrometer (295-492 nm, grating #10, 1800 lines mm^{-1}, 2048 element CCD, 25µm slit, UV2 upgrade, L2 lens, 0.5 nm resolution) and spectra were acquired using Spectrasuite software.

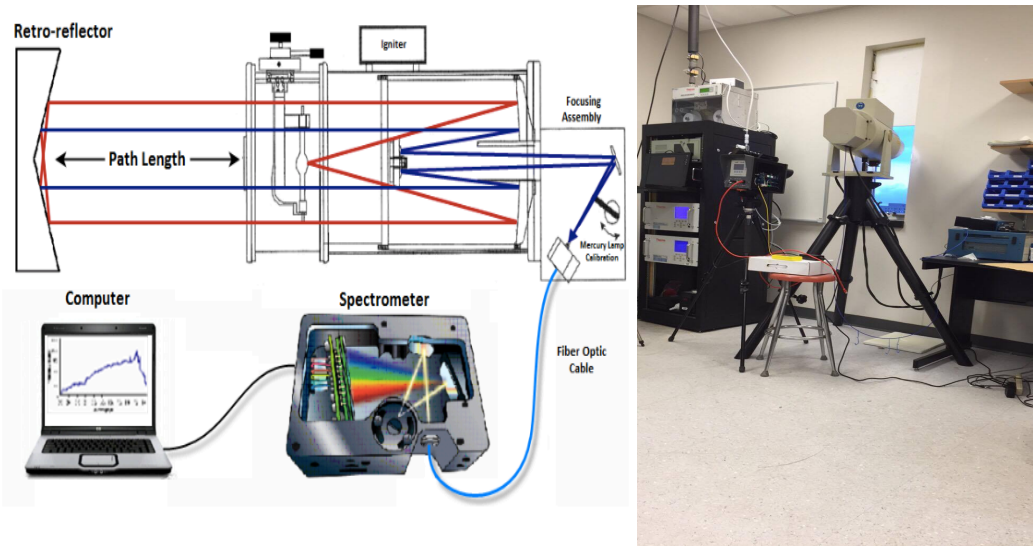

Figure 9: **Left:** Schematic of the DOAS system instrumental setup. The paths for the outgoing and incoming beams are shown in red and blue, respectively. **Right:** A modified DOAS 2000 Instrument (TEI Inc.).

2.2.2.2- Analytical study of active-DOAS

The detection limit of active-DOAS for SO_2 had to be determined in order to ensure that detecting a ship plume is possible in a given time period with the use of our set up. In this section a SO_2 sample cell was used for a predictable measurement of absorption. SO_2 measurements were performed using the 10 ppm-m SO_2 sample cell along with a low pass quartz filter (purchased from Edmund Optics with diameter of 25 mm and high wavelength cut-off at 400 nm) in order to minimize stray light effect. Stray light (false light) inside a spectrometer is the light being detected that does not belong to the bandwidth of the chosen wavelength interval. Light scattering and diffraction of the instrument causes the effect of stray light that causes a decrease in the measurable absorbance range and reduces the linear relationship between concentration and absorbance of the instrument. Stray light can be a problem at any wavelength. As a result, filters are needed which would ideally reject all light not in the chosen desirable wavelength range. The SO_2 sample cell was placed in the return beam path on the filter as shown in Figure 10.

The measurements were performed on three different days (5th December 2016, 22nd January 2017 and 6th February 2017) with the same measurement, calibration and fitting procedure. The 30-cube Al retro-reflector was used with a return path length of 498 m. In total, 107 spectra were collected with an integration time of 150 ms each and 40 averages that took nearly 10 minutes while the time for each averaged spectrum is 6 seconds. The reason for selecting the 150 ms and 40 averages was to determine the detection limit at our target measurement time (6 sec), which would be necessary in order to capture a 2-minute transient plume with 20 measurement points. Twenty points is seen as a good target for capturing chromatographic peaks in HPLC or GC (Skoog *et al*., 1998). Also, offset, dark current, Xe-lamp and mercury lamp spectra were collected. Spectral analysis software and spectral fitting procedures were used that are explained in detail in the following sections.

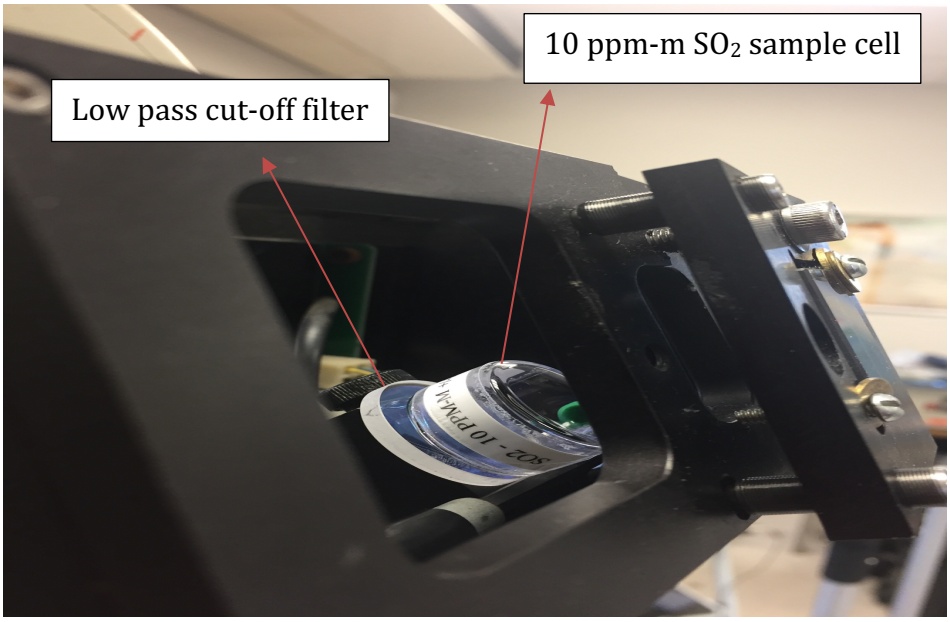

Figure 10: The orientation of filter and 10 (ppm-m) SO_2 sample cell in front of the fiber optic. In this picture, the cell is placed on top of the filter

2.2.2.3- Electronic offset and dark current

Offset

An offset spectrum was taken in order to account for an artificial background electronic signal produced within the spectrometer. This was achieved by removing the fiber from the active-DOAS and capping the end of the fiber cable to block all incoming light to the spectrometer. An offset consists of the positive baseline signal produced during data sampling and depends specifically on the detector electronics. By subtracting this baseline, we ensure that the signal intensity being fit is associated with photons projected and received by the telescope. Offset corrections were applied to the data prior to the fit procedure by subtracting the temperature specific offset from each ambient spectrum, lamp spectrum and Hg spectrum. Offset spectra were collected with an integration time of 30 (ms) and 10000 spectral averages (Figure 11). In addition, since the electronic offset reveals a negative dependence with temperature, it must be collected at the same

detector temperature as all other spectra. Therefore, a Resonance Ltd temperature controller was used to maintain the spectrometer temperature at 10 °C.

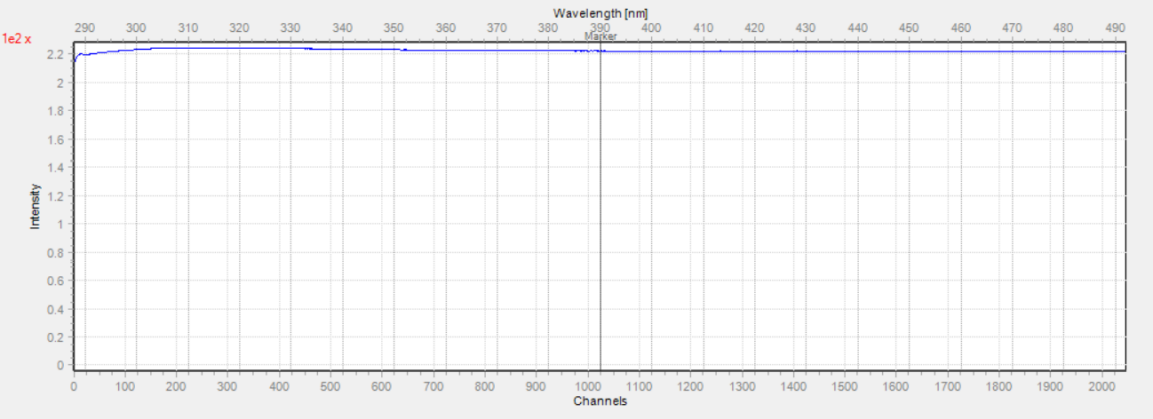

Figure 11: Sample offset spectrum collected on 22nd January 2017 using the USB2000 spectrometer with integration time of 30 ms, 10000 averages and temperature controller stabilized at 10°C.

Dark Current

Dark current is the variable response obtained by the detector in the absence of light. This pixel-to-pixel variation is caused by the thermal noise within the detector CCD elements, and is positively correlated with temperature. Dark noise is element specific and is proportional to the integration time. In contrast to the offset, dark current increases with the exposure time of the measurement as increasing the exposure time increases the available time for hot electrons to be excited. The detector was kept at the same temperature as the measurements using the temperature controller. Ideally measurements are made at a low temperature to reduce dark current and the dark noise associated with the dark current. The

measured dark current spectrum was subtracted from the lamp and measured ambient spectra prior to the fit procedure. This was achieved by multiplying the dark current spectrum by a ratio of the

integration time used on the sample over that used for the dark current spectrum. If temperature fluctuations are present during the measurements, then the dark current spectrum can be included as an additional species in the fit scenario, removing its features from the collected spectra. Therefore, dark current and offset spectra should be collected daily or at the beginning and end of the measurement period at the same temperature as the other spectra. Dark current spectra were collected with 15000 (ms) integration time and 30 spectral averages (Figure 12). It is necessary to note and account for the differences in integration time of dark current spectrum and the integration time of the ambient/lamp spectra.

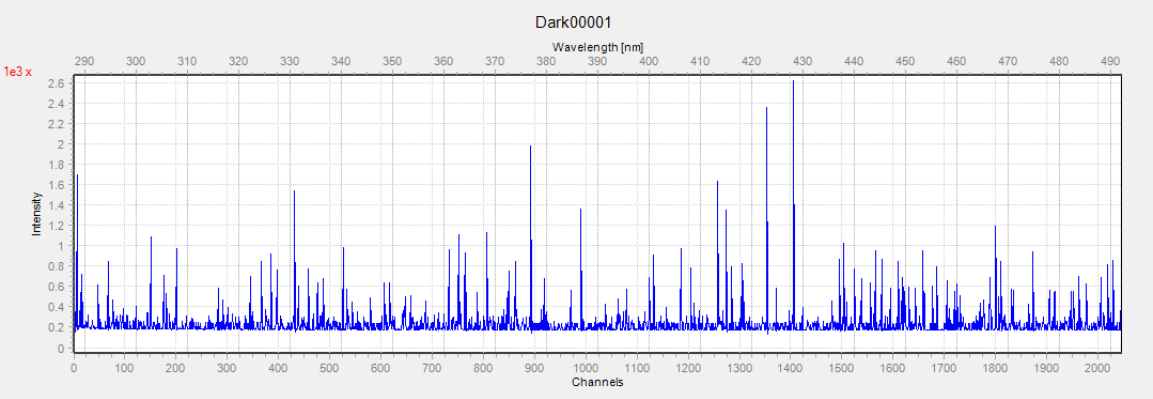

Figure 12: Sample dark current spectrum collected on 22nd January 2017 using the USB2000 spectrometer with integration time of 15000 ms, 30 averages and temperature controller stabilized at 10°C.

2.2.2.4- Xenon-arc Lamp Spectra

A sample lamp spectrum is shown in Figure 13, with an integration time of 100 ms and 8000 averages using the USB2000 spectrometer. The lamp spectrum consists of a sum of thermal emissions according to Planck's law with broadened emission lines due to pressure and temperature. The xenon lamp reference spectrum was collected (Figure 13) by adjusting the optics

of the DOAS system to direct some random scattered light emitting from the lamp directly into the fiber optic, without it traversing through the open atmosphere.

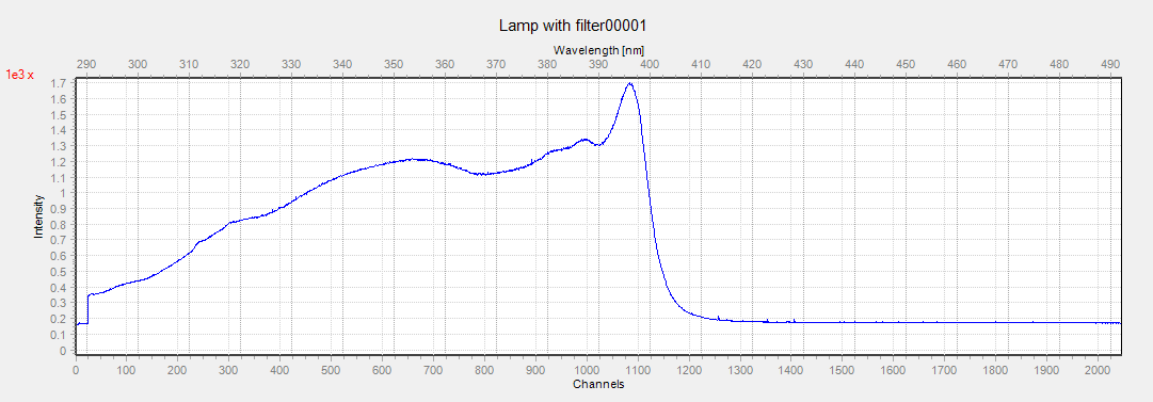

Figure 13: Sample lamp spectrum collected on 22nd January 2017 using the USB2000 spectrometer with integration time of 100 ms, 8000 averages and temperature controller stabilized at 10°C.

2.2.2.5- Mercury Lamp Spectrum and Spectral Convolution

A mercury lamp spectrum was needed for wavelength calibration and spectral convolution of reference spectra to match the slit function of the spectrometer. An integration time of 100 (ms) and 8000 spectral averages were used (Figure 14). The mercury spectrum was collected by aiming the light of the Hg lamp on to one spot of a clear white paper and focusing the end of the fiber optic cable on this point while blocking all other external light. Calibration lines were collected by using light sources from mercury lamp. These peaks allow for each sample spectrum collected to be corrected for any wavelength shift as a result of temperature changes in the spectrometer. The main wavelength calibration peaks used in this set of experiments were at 334.15, 313.17 and 302.15 (nm).

The mercury lamp had its calibration applied to the sample spectra after the offset and dark noise were subtracted. The Hg cross-sections used were obtained from various published sources. They were convoluted using a convolution kernel into a blank spectrum which had been calibrated with the mercury lamp data. This convolution corrected for the differences between the spectrometer

used to collect the reference cross-sections (Bogumil *et al*., 2003) and the spectrometer used to collect the sample spectra. In essence, the convolution process matches the wavelength resolution of the reference SO_2 spectra, and their differential cross sections, to be equal to the wavelength resolution of the spectrometer at the temperature used for the measurements of ambient spectra.

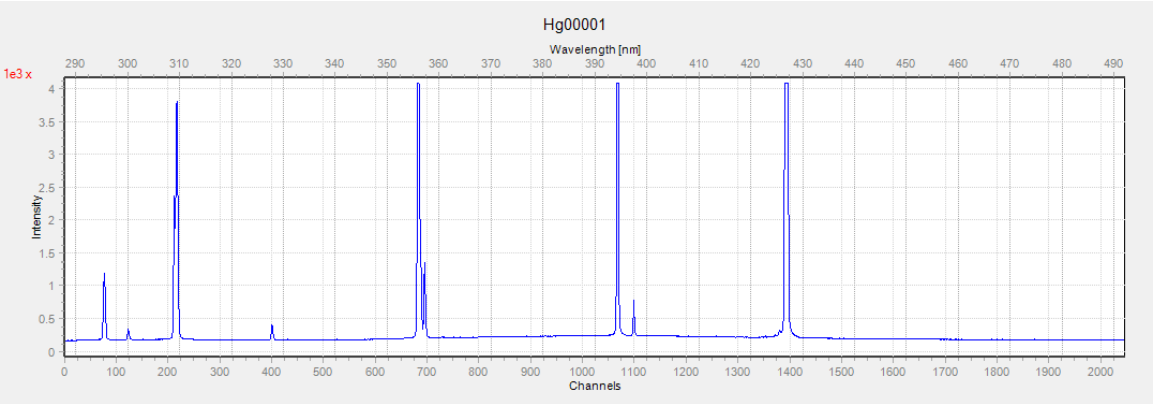

Figure 14: Sample xenon lamp spectrum taken on 22nd January 2017 using the USB2000 spectrometer with integration time of 100 ms and 8000 averages and temperature control stabilized at 10°C.

2.2.2.6- Spectral Fitting Procedure

The measured ambient spectra can be corrected and analyzed using DOASIS software (Kraus, 2006), that uses Levenberg-Marquardt algorithm to numerically solve the non-linear systems (Levenberg, 1944). The algorithm uses an iterative approach to obtain a continuously improved estimate for the model parameters with each iteration until the optimal solution is found. The method consists of a least square fit in which a linear component is used for retrieval of the trace gas absorption in combination with a non-linear component, accounting for spectral shifts between the measured and chosen reference spectra to reduce the residual of the fit. In order to perform a fit, the software requires a predefined fit scenario, consisting of the lamp spectra and all the species present in the light path with significant absorption features within the chosen wavelength range (302 – 312 nm). This region should include distinct peaks in the cross-section of the gas chosen to

fit. The region should also not have any other significant features from the lamp. The fit scenario included a convoluted absorption cross-section spectrum of NO_2 (Bogumil (2003) 293K [NO2]), SO_2 (Bogumil (2003) 293K_SO_2), a mercury lamp spectrum and a 2^{nd} order polynomial. Details of the fit scenario used for the spectral analysis of the active-DOAS are summarized in Table 2. Figure 15 indicates the convoluted differential SO_2 spectra used for fitting. The optimal wavelength interval for SO_2 fitting procedure is 302-312 nm since the SO_2 cross-section has unique features within this wavelength range and there are not many other trace gasses at high concentrations that have absorption within this wavelength range. Due to unique features and high absorption cross section of SO_2 within 302-312 nm, separation of absorption is possible and will show high optical densities and the sensitivity improves in this wavelength region. In order to analyze the data, a Jscript program was used to automate the fitting process. Upon completing the algorithm, the software computes a slant column density and a fit error for each trace gas within the selected fit scenario. Then, the mixing ratio for a given species is calculated post analysis given the path length of the light beam and the number density of the air mass for a specific temperature and pressure. All broadband features were combined together and separated from the narrowband features by fitting a polynomial to the broadband features of a collected spectrum. The order of the polynomial was chosen based on the shape required, often 2nd or 3rd. This polynomial accounts for the broad band attenuation due to Rayleigh scattering, Mie scattering and instrumental effects (Platt et al, 1979). The difference between the actual spectrum and the fit is calculated. This minimum value can be found using a least square fit (Stuttz and Platt, 1996). For a successful retrieval, all the absorption features of the trace gases that had strong differential features in the fitting range had to be present. The residual is effectively the difference between the measured spectrum and the modeled spectrum. The size of the residual can be used to indicate the quality of the fit. A stronger fit is the one, which has a lower residual value. Errors in the fit can arise due to failing to include

the absorption cross section of a gas that is significantly absorbing. The software then applies shift and squeeze to find the best fit of the cross-section to the spectrum. These values are all then reported and used for the calculation of gas mixing ratios.

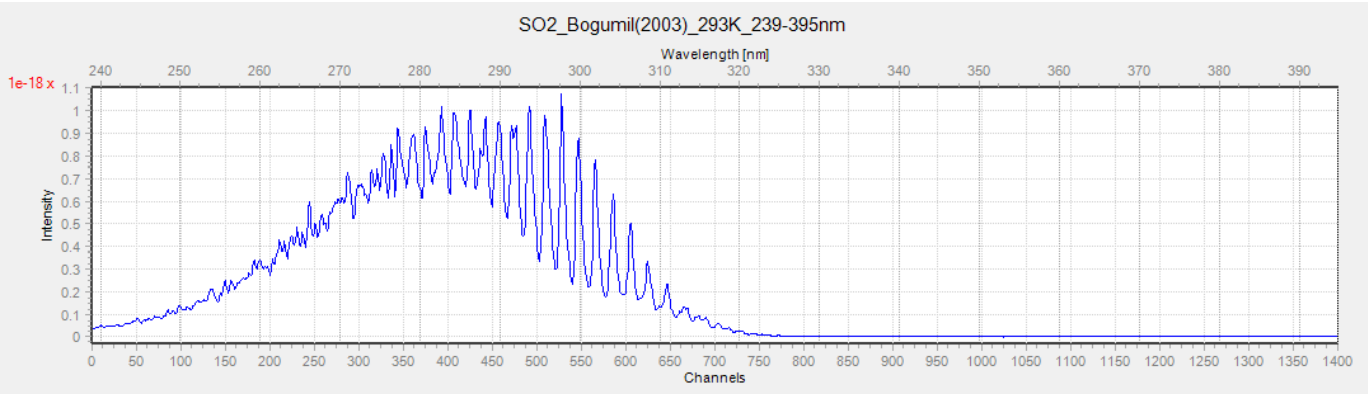

Figure 15: The convoluted differential SO_2 spectra used for fitting at 293k.

Table 2: Details of the fit scenario used for the spectral analysis of the active-DOAS data

Fit constituent	Reference
Mercury lamp	From measurement
Lamp spectrum	From measurement
Dark current	From measurement
Offset	From measurement
SO_2	Bogumil (2003) 293K_SO_2
NO_2	Bogumil (2003) 293K_NO2
2nd order polynomial	Fitted by DOASIS
Fit range SO_2 retrieval	302.0-312.0 nm

Figures 16a, 16b and 16c indicate the SO_2 fit coefficient versus the spectrum number retrieved from 107 spectra on three days. The average, standard deviation, detection limit (3σ) and quantification limit (10σ) of SO_2 fit coefficients for each day were calculated and summarized in

Table 3. In addition, the SO_2 cell concentration was calculated and converted in ppm-m unit in order to compare it with true cell concentration, which was nominally 10 ppm-m. As can be observed in Table 3, the lowest detection limit (3σ) and quantification limit (10σ) were 4.2×10^{15} and 1.4×10^{16} $\mathrm{Molecule.\,cm^{-2}}$, respectively that are from 22nd January 2017. Therefore, these values are the lowest possible slant column density values (SCD) values that active-DOAS could measure for SO_2. We need to compare these values with SCD values we expect as a beam crosses a real transient ship plume. We looked at values in literature to determine what SCD values are to be expected in real ship plumes with moderate fuel sulfur content. Then, we are able to decide whether active-DOAS is a suitable instrument for this project or not. In a report by Berg *et al*. (2010), a MAX-DOAS system performed SO_2 measurements using reflected solar light. In this study, an aircraft, which was at a few hundred meters altitude, moved in such a way that the field of view of the optical telescope transects the plume of interest coming from a ferry that had known sulfur fuel content of around 1.0%. A SO_2 SCD of 2.25×10^{16} $\mathrm{Molecule.\,cm^{-2}}$ was yielded. Also, Schreier *et al*. (2014) reported the SO_2 slant columns measured by a ship-based MAX-DOAS instrument in the coastal and open waters of the South China and Sulu Sea. This study found elevated values of SO_2 SCDs exceeding 2×10^{16} $\mathrm{Molecule.\,cm^{-2}}$ at $\alpha=2°$ when the ship loaded with the MAX-DOAS was moving in proximity to the dense shipping lane. These measurements were performed in the proximity to the individual ships and thus, reflected rather fresh emission plumes. Unfortunately, this study did not mention any details about the levels of sulfur in the fuel, the type and size of the marine vessels. These values obtained from literature are higher than the detection limit and similar to the quantification limit determined for our active-DOAS measurement in a 6 second period. Therefore, it is concluded that capturing a ship plume and retrieving the SO_2 column with 6-second time resolution in a marine area is feasible with the use of our instrumental set up.

Table 3: Average fit coefficients; SO_2 cell concentrations in ppm-m, standard deviation, detection and quantification limits were calculated for SO_2 sample cell with the filter on three different days.

Date	Average Fit coefficient ($\mathbf{Molecule.\,cm^{-2}}$)	SO_2 cell concentration (ppm-m)	Standard deviation of Fit coefficient ($\mathbf{Molecule.\,cm^{-2}}$)	Detection limit (3σ)	Limit of Quantification (10σ)	Average fit error ($\mathbf{Molecule.\,cm^{-2}}$)	Standard deviation of fit error ($\mathbf{Molecule.\,cm^{-2}}$)
5.Dec.2016	2.15×10^{16}	8.74	3.2×10^{15}	9.7×10^{15}	3.2×10^{16}	5.0×10^{15}	3.4×10^{14}
22.Jan.2017	2.01×10^{16}	8.17	1.4×10^{15}	4.2×10^{15}	1.4×10^{16}	3.1×10^{15}	1.4×10^{14}
6.Feb.2017	2.19×10^{16}	8.90	2.0×10^{15}	6.1×10^{15}	2.0×10^{16}	2.4×10^{15}	2.1×10^{14}

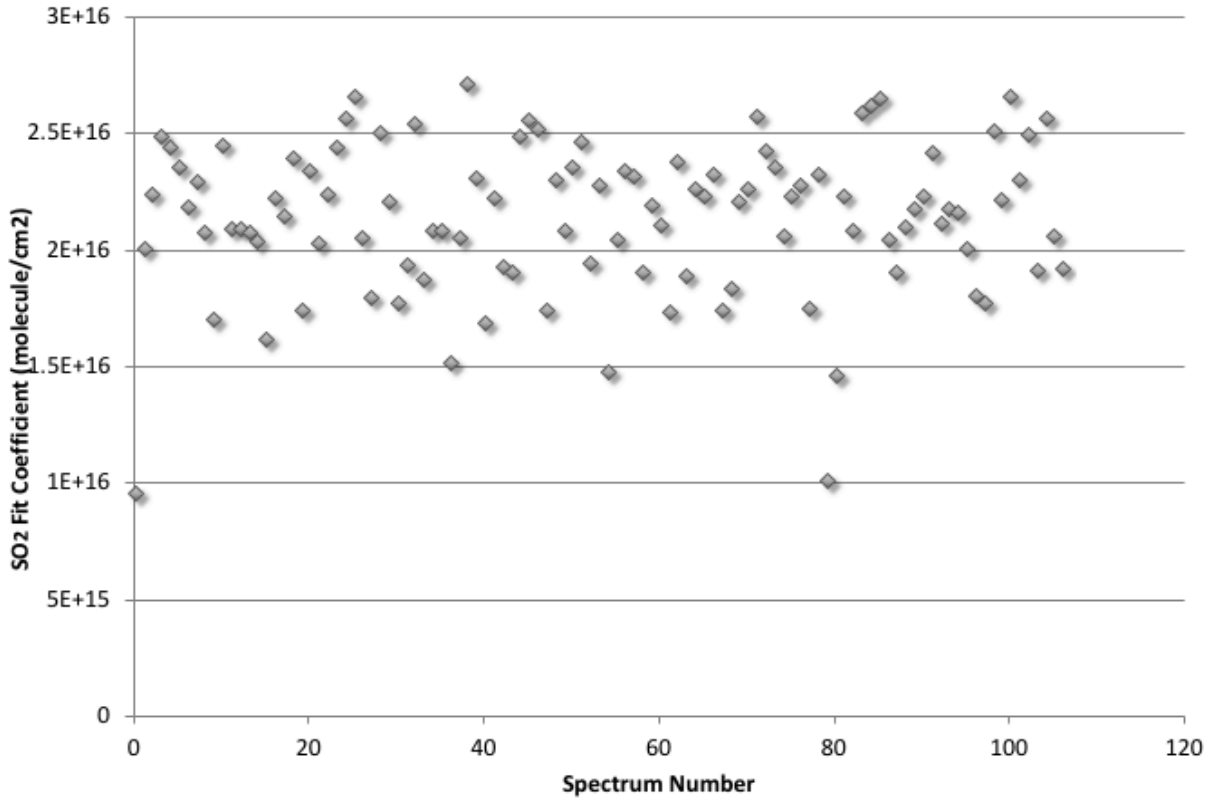

Figure 16.1: SO_2 fit coefficient versus spectrum number for 10 ppm-m SO_2 sample cell with cut-off filter on top for the fitting range of 302-312 (nm). 107 spectra were collected on 5 Dec 2016 for about 10 minutes while each spectrum takes 6 seconds to be collected. Integration time =150 ms, $N_{avg} = 40$.

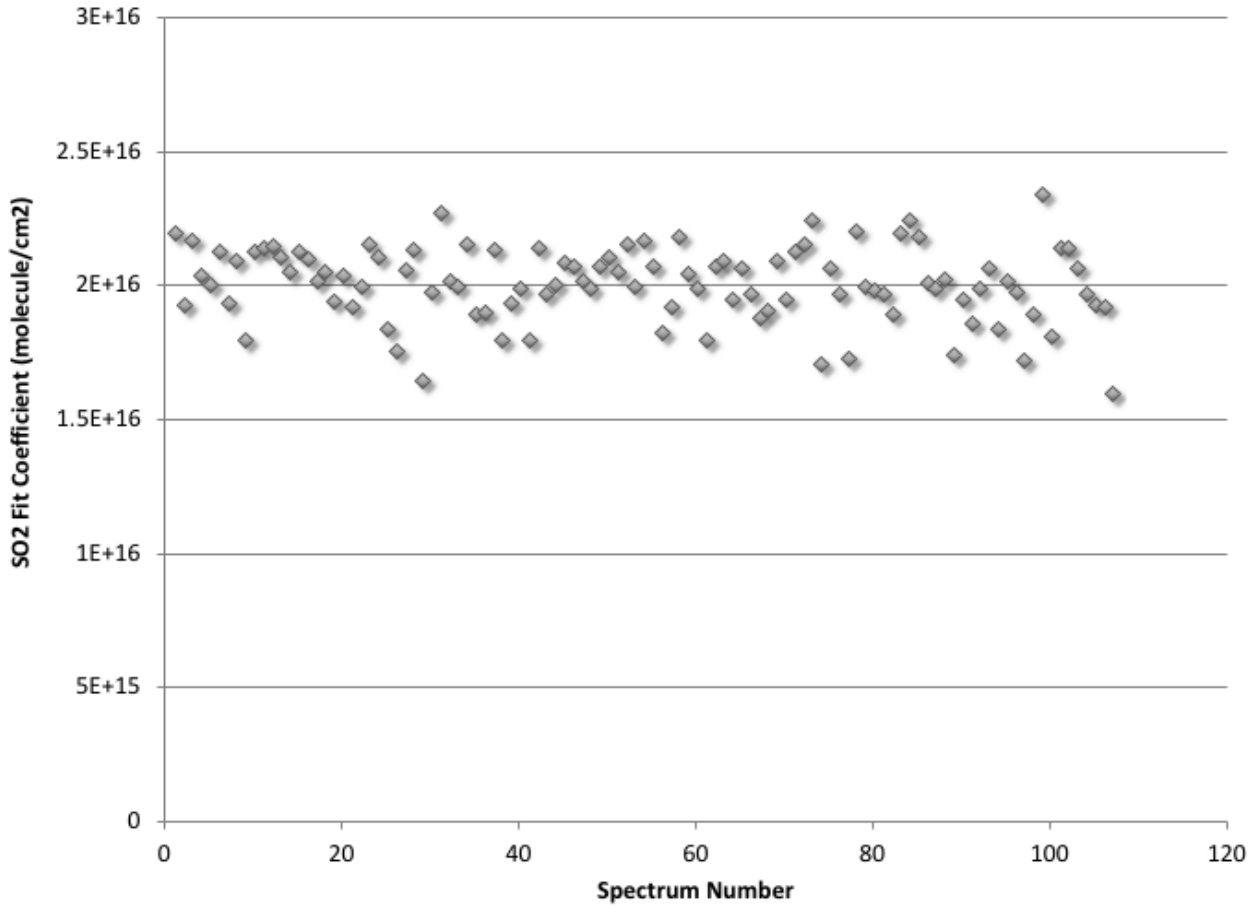

Figure 16.2: SO_2 fit coefficient versus spectrum number for 10 ppm-m SO_2 sample cell with cut-off filter on top for the fitting range of 302-312 (nm). 107 spectra were collected on 22 Jan 2017 for about 10 minutes while each spectrum takes 6 seconds to be collected. Integration time =150 ms, $N_{avg} = 40$.

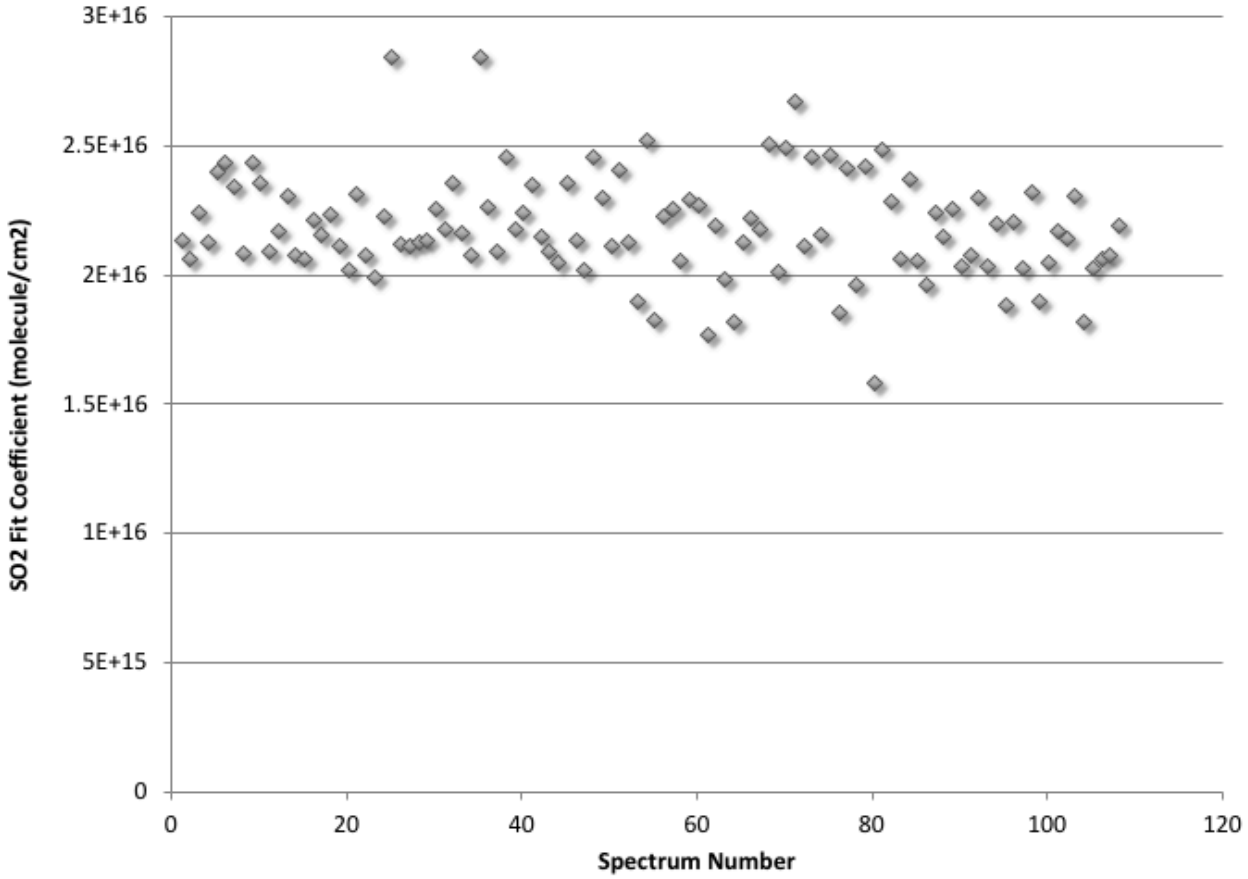

Figure 16.1: SO_2 fit coefficient versus spectrum number for 10 ppm-m SO_2 sample cell with cut-off filter on top for the fitting range of 302-312 (nm). 107 spectra were collected on 6 Feb 2017 for about 10 minutes while each spectrum takes 6 seconds to be collected. Integration time =150 ms, $N_{avg} = 40$.

2.3- Field Experiment

Our goal was to establish an absorption path close to a well-frequented waterway utilizing our two instruments. Active-DOAS and TDLAS were side by side with their beams transecting the same air mass, hopefully capturing a ship plume. For this project, continuous measurements of SO_2 and CO_2 mixing ratios were made as ships passed by in the polluted Welland Canal environment. Information about the marine vessels, such as their size and arrival times, were obtained from the Saint Lawrence seaway website. The name of marine vessels and their arrival times to the experiment site were recorded in order to attribute them with their corresponding peaks. In order to characterize the SO_2/CO_2 ratio from pollution sources, 5 plume events were identified. Then, the SO_2/CO_2 ratios were determined using two related methods: 1- Linear least squares regression of SO_2 to CO_2 and 2- Calculating the integrated excess pollutants (Δx) during the plume event. The mass-based emission factors (g of SO_2 emitted per kilogram of fuel consumed) for these two techniques were calculated using the SO_2/CO_2 ratios and eventually the percentage of sulfur in the fuel was determined.

2.3.1- Location and meteorology

The ship plume field study took place on July 31st and 1st August 2017 next to the Welland Canal. The Welland Canal is located in the Niagara region of Ontario, Canada between two of North America's great lakes, Lake Ontario (75 meters above sea level) and Lake Erie (174 meters above sea level). The Welland Canal is a vital link in the St. Lawrence seaway passage from the Atlantic Ocean to Midwestern Canada and the United States. The canal is about 43.4 kilometers in length and includes seven lift locks that bring vessels up an elevation of 99 meters from Lake Ontario to Lake Erie. The Welland

Canal is important because of its ability to move ships full of cargo up and down the Niagara Escarpment which contributes to the economic growth. A map of the Welland Canal is shown in Figure 17 where the study area is circled.

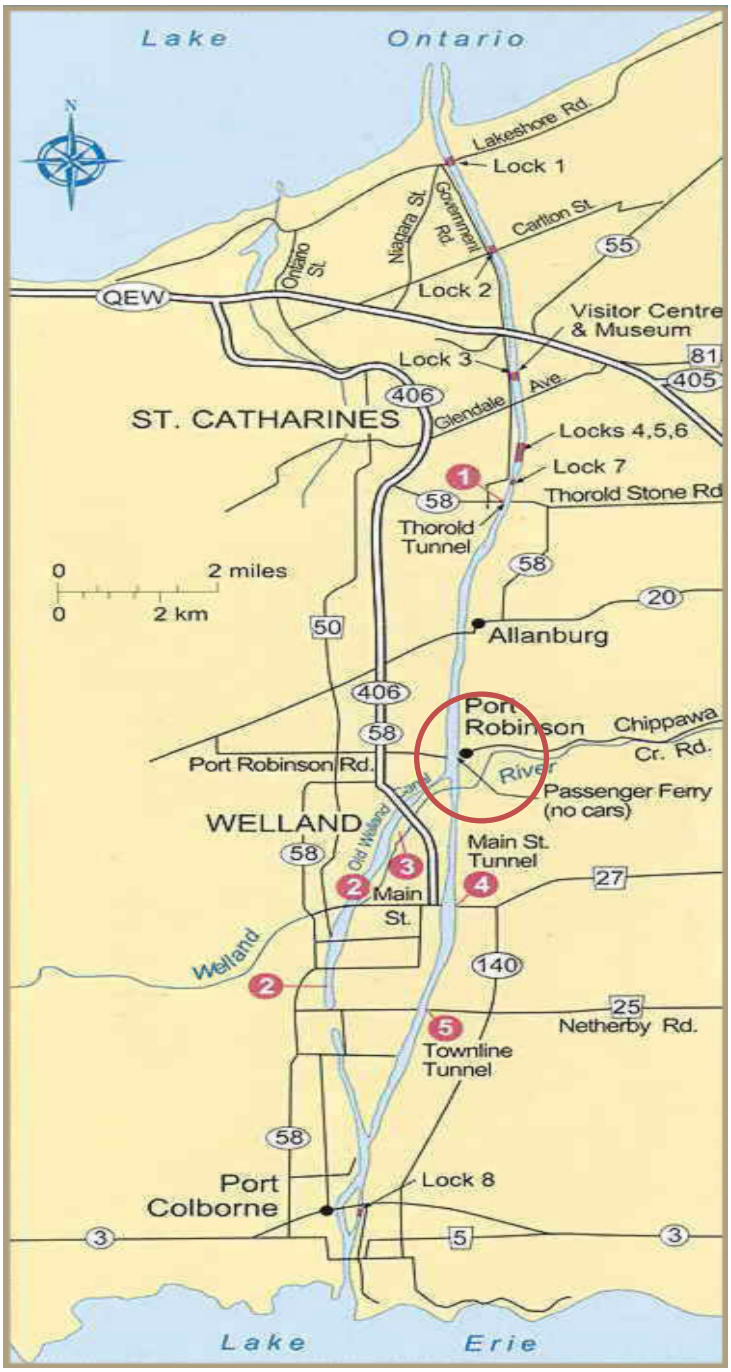

Figure 17: Welland canal map. The location of the study is indicated with a red circle on this map.
http://www.infoniagara.com/attractions/welland_canal/canal_map.aspx

A map of the study area is shown in Figure 18 with the locations of the instruments and retro-reflectors indicated. The TDLAS and active-DOAS were positioned side by side within close proximity (less than 2 meters apart). They were located about 200 meters away from the East side of the Welland Canal nearby a grassy area with altitude of 10 meters above the water level. A 30-cube aluminum enhanced and a 23-element gold retro-reflectors were utilized to return the beams from active-DOAS and TDLAS, respectively. The path length between instruments and retro-reflectors was measured with a Garmin GPS to be 289.7 meters, leading to a total absorption path length of 579.4 meters. Figure 19 shows a picture of the retro-reflectors located side by side, less than a meter a part. The geographical coordinates of instruments and retro-reflectors and the altitudes above water level of the canal are summarized in Table 4. This study dealt with the exhaust emitted from ships' smoke stacks. Therefore, it was important to choose a location that is a representive of the marine plumes and equally be far away from other strong emission sources, which is typical for a city area. The instruments were located on the East side of the canal so that with suitable West winds plumes from ships are transported into the beam path of the instruments. Choosing a location for studying air pollution is challenging, as there is always a compromise between practical and theoretical limitations. Unfortunately, our study area was impacted by the plumes emitted from trucks passing-by (Trafficking in Biggar Rd and River St). Prior to the experimental procedure we were not aware of the amount of truck traffic. The truck emissions caused some difficulties in distinguishing ship plumes from truck plumes when analyzing the data. In addition to ship's arrival time, the arrival times of trucks were also recorded. Therefore, identifications of plumes associated with marine vessels

would be more efficient. The days July 31st and 1st August 2017 were specifically chosen for this study as this study depended on the prevailing wind to transport the plume to the beams. The wind direction for these days were 9km/h West and 6km/h Southwest, respectively. Also, the

temperature for these days were 27°C and 24°C, Respectively. The Port Robinson weather network was used for wind speed, wind direction and temperature information. On 1st August 2017 the wind direction changed dramatically towards the end of the measurement period, as a massive cloud (thunderstorm) created an updraft and change in wind direction, carrying the plumes west of the canal.

Table 4: Coordinates and headings of the instrument.

Instrument	Coordinates	Altitude above water level of the canal (m)
Active-DOAS and TDLAS	°N43.026974 °W79.208562	10
30-cube and Gold retro-reflectors	°N43.029247 °W79.210428	30

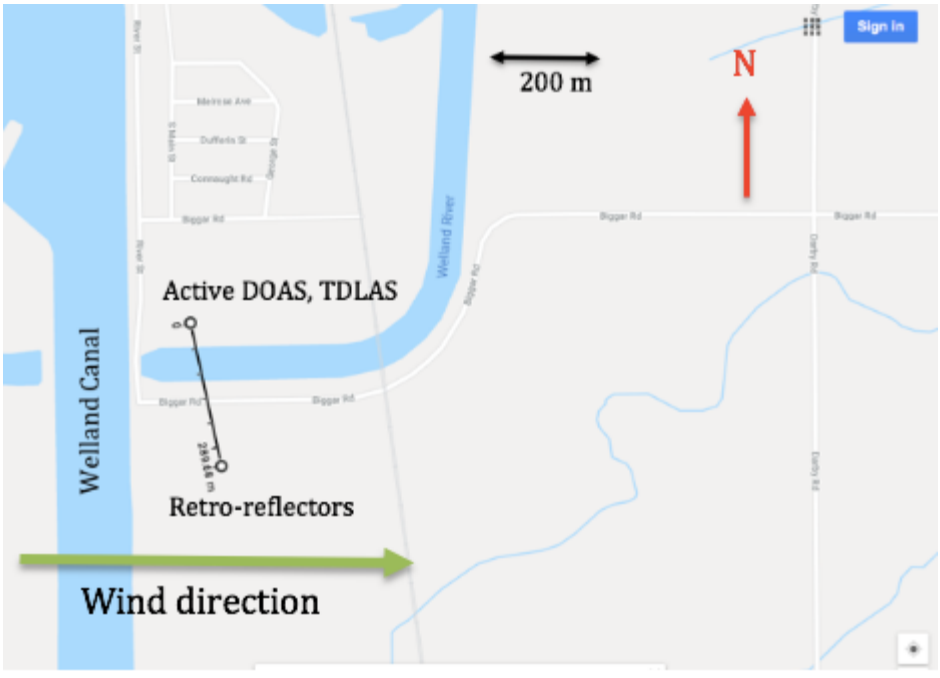

Figure 18: Map of the study area showing the location of instruments and retro-reflector.

Figure 19: (On the Left): Active-DOAS and TDLAS are side by side and pointing to retro-reflectors that are 289.7 meters away (On the right).

2.3.2- Identification of ships

In this study, marine vessels could be seen approaching the measurement site. The Saint Lawrence seaway website (http://www.greatlakes-seaway.com/en/navigating/map/index.html) was used to identify the ships in the Canal. This website includes a seaway map with the schedule for marine vessels in the canal as well as the vessel's name, size, current location, next destination and estimated arrival time. The arrival time of ships observed at the measurement site on 31st July and 1st August 2017 along with their size and their directions are summarized in Tables 5 and 6, respectively. Moreover, the schedule for trucks passing the measurement site on 1st August 2017 is also recorded in Table 6. Unfortunately, the Trucks' schedule for July 31st was not recorded since the impact of the truck plumes on the measurements was underestimated at the beginning of the study and this made it difficult to assign the ships to the plumes and perform further data analysis

for this day. As can be seen from both Tables 5 and 6, the passage for each vessel is indicated as up or down bound. Up-bound is the passage moving up the locks from Lake Ontario to Lake Erie. Down-bound is moving down the locks from Lake Erie to Lake Ontario.

Table 5: The schedule for ships passing by the measurement site on 31st July 2017. The marine vessels size and the direction of the ships transiting are summarized in this table.

Time	Vessel	Direction	Width (m)	Length (m)
12:25 PM	Federal Kiva	Up bound	23.8	200
13:28 PM	Pear Mist	Down bound	16.8	99.0

Table 6: The schedule for ships and trucks passing by the measurement site on 1st August 2017. The marine vessels size and the direction of the ships transiting are summarized.

Time	Vessel	Direction	Width (m)	Length (m)
11:20 AM	Truck			
12:09 PM	Truck			
12:11 PM	Truck			
12:37 PM	Coast guard	Down-bound	~7	~5
12:58 PM	CSL Assiniboine	Up-bound	23.8	225.5
1:46 PM	Truck			
2:38 PM ***Wind shifted**	Truck			
2:43 PM ***Wind shifted**	CSL Welland	Up-bound	23.8	225.5
2:50 PM ***Wind shifted**	Algonova	Down-bound	19.8	129.9

2.3.3- Instrumental set-up

For this project, time series of SO_2 and CO_2 mixing ratios were measured as ships passed by in the polluted Welland Canal environment. Both TDLAS and active-DOAS were run on July 31st and 1st August 2017 from 12:19:00 pm to 1:45:00 pm and 10:45:00 am to 2:50:00 pm, respectively. The instruments were started and warmed up for two hours prior to the measurement. TDLAS measured CO_2 mixing ratios. The laser beam was aligned in a way to receive the maximum possible return signal intensity from the 23-element gold retro-reflector. A Yeti 400-watt battery pack was used to power TDLAS.

Active-DOAS measurements of SO_2 were collected using the low-pass quartz filter (cut-off at 400 nm). The telescope was aligned to receive maximum return light intensity. A resonance Ltd temperature controller system was used to maintain the spectrometer's temperature at 20°C. Auxiliary spectra including the offset, dark current, lamp and mercury lamp were collected, as described previously (2.2.2- Analytical work of active-DOAS for SO_2 measurements). Information for integration time and number of averages for measurement spectra are summarized in Table 7. A Honda EU1000i portable gas-powered generator with AC power inverter was utilized to power the active-DOAS. The generator was located downwind from the instruments to the east (~ 20 meters) to ensure the emissions from the generator did not intersect the beam path of the optical instruments.

Table 7: Integration time and number of averages used for collecting the measurement spectra using the Spectrasuite software.

Spectra	Integration time (ms)	Number of averages
SO_2	60	100
Lamp spectra	60	2000
Mercury lamp	100	8000
Dark current	5000	15
Offset	30	10000

3- Field Work Results and Discussion:

3.1- 31st July 2017 Results

The DOASIS software was used for retrieving the SO_2 column densities from the collected spectra. The fitting scenario for SO_2 included differential cross sections of SO_2 (Bogumil *et al*., 2003) and NO_2 (Bogumil *et al*., 2003) and 2nd order polynomial fit to the broadband features of the spectrum. The column density of SO_2 was calculated using a fitting range of 302.0-312.0 nm and the fit coefficients were converted to mixing ratios. Each data point had a collection time of 6 sec (nominally) as the SO_2 spectra were collected with an integration time of 150 ms and 40 averages. However, SO_2 measurements were not exactly every 6 s due to delays in data download and storage from the spectrometer to the computer, resulting in 6-7 sec time intervals. SO_2 mixing ratios were stacked in to groups of 5 data points. Then, the Exponentially Weighted Moving Average (EWMA) technique was performed on each group of the data points in order to smooth the noise, so that we are able to observe a trend in SO_2 mixing ratios.

The TDLAS instrument measured CO_2 mixing ratios with 5.0 second dwell time. Based on previous analytical work performed at York University (Section 2.2.1), it was concluded that post averaging the data collected at short dwell times is possible and desirable in cases where the length of the transient plumes is not predictable in advance. We had realized that we needed to use small dwell times for the field experiment in order to ensure that we are able to capture the temporal transient of a plume and observe an increase in CO_2 mixing ratios before the plume diffuses. However, mistakenly the desired 0.1 second dwell time had not been saved in the TDLAS setting and CO_2 measurements were taken with 5.0 second which is the default dwell time of the instrument.

Figure 20 shows SO_2 and CO_2 mixing ratios measured during the field experiment. The marine vessels are labelled on the graph. As can be observed from Figure 20, there are no increases in CO_2 or SO_2 mixing ratios associated with the arrival time of the marine vessels. For example, the vessel Federal Kiva reached the experiment site at 12:25 PM. However, there are no increases in CO_2 or SO_2 mixing ratios around this time. Looking at Figure 20, there are no increases in CO_2 or SO_2 mixing ratios at 13:28 which is the arrival times of Pearl Mist vessel. It is important to note that the first indication of a plume is observing an increase in CO_2 mixing ratios. However due to the large dwell time of TDLAS, it is not possible to identify increases in CO_2 mixing ratios and no plume-related trend is observed in CO_2 data. Also, the vessels Federal Kiva and Pear Mist could be running on a very low Sulphur fuel which is consistent with the low Sulphur compliance. As a result, active-DOAS was not able to detect the SO_2 from the marine vessel plumes and that is why there are no indications of a plume in SO_2 trends. To add more, it is not certain that the fluctuations are arising from the ship plume and not the truck plumes as trucks were passing by the experiment site frequently during the measurements. Regrettably, the trucks' schedule was not recorded on this day, impeding our ability to distinguish between truck plumes and ship plumes on July 31st.

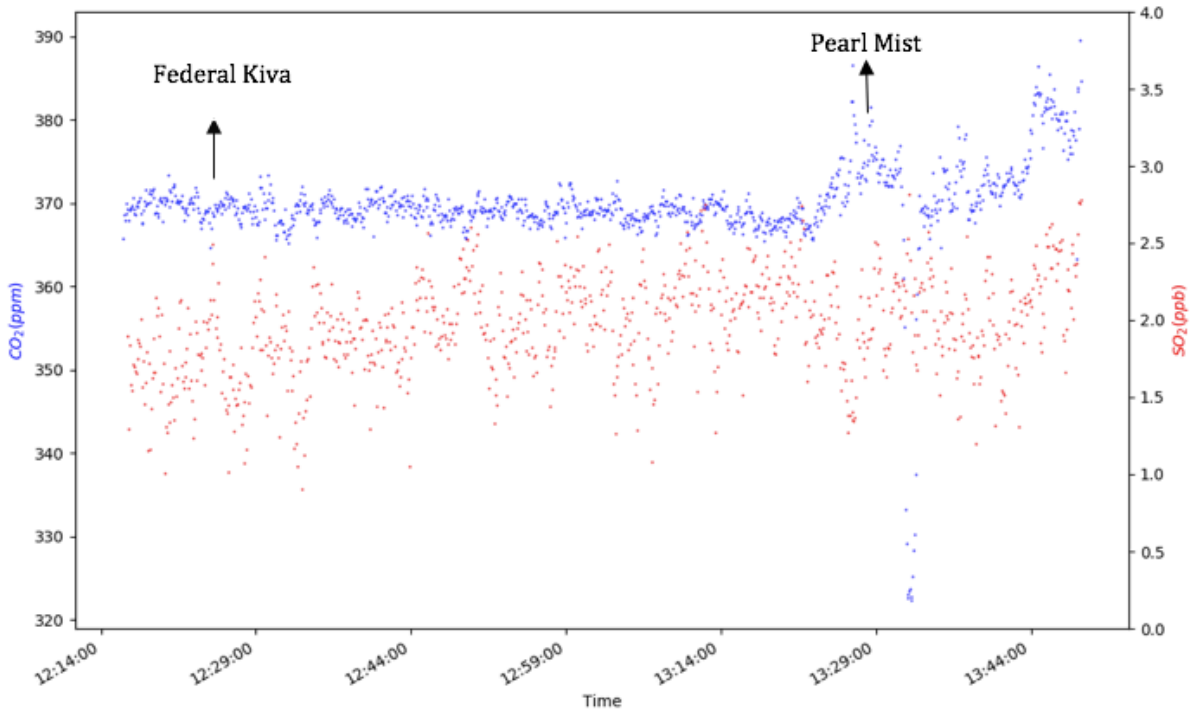

Figure 20: SO_2 and CO_2 mixing ratios versus time graph for July 31, 2017. CO_2 and SO_2 measurements were taken with 5.0 and 6.0 seconds dwell time, respectively. SO_2 data points are smothed using EWMA technequie.

3.2- Aug 1, 2017 Results

For this day, each SO_2 data point had a collection time of 6 sec (nominally) as the SO_2 spectra were collected with an integration time of 150 ms and 40 averages. Also, TDLAS instrument measured CO_2 mixing ratios with 0.1 second dwell time. First, both CO_2 and SO_2 mixing ratios were stacked into groups of 5 data points. Then, the Exponentially Weighted Moving Average (EWMA) technique was performed on each group of the data points in order to smooth the noise. SO_2 data points were averaged to 30 seconds and the CO_2 data points were averaged to 0.5 second. This technique averages the data in a way that causes less weight to the data as they are further removed in time. The "weighted" choice makes the moving average less sensitive to minor drifts in the process. The schedule for trucks passing the measurement site was recorded for this day which guided us to distinguish between peaks associated with ship plumes and truck plumes.

Figure 21 shows times series of SO_2 and CO_2 mixing ratios measured during the field experiment. By comparing Figures 20 and 21, it is evident that variation in CO_2 mixing ratios is more observable in Figure 21. Therefore, measuring CO_2 mixing ratios with 0.1 second dwell time played an important role in identifying CO_2 peaks resulting from each plume event. As can be seen from Figure 21, amongst all the marine vessels observed on Aug 1, 2017, the marine vessels that caused observable increases in the CO_2 and SO_2 mixing ratios were the coast guard and CSL Assiniboine. Unfortunately, the wind direction changed dramatically towards the end of the measurement period, as a massive cloud (thunderstorm) created an updraft and developed significant wind and change in wind direction, carrying the plumes west of the canal. Therefore, distinguishing peaks associated with a truck, the marine vessels CSL Welland and Algonova is not possible for the time period of 14:20 and onwards. Moreover, CSL Welland and Algonova were approaching the measurement site almost at the same time from opposite directions (one south bound, the other north bound) and this incident made the plume analysis even more difficult for that time interval. Overall, ship emissions did not result in dramatic increases in CO_2 mixing ratios in comparison to truck emissions, which created comparable increases in CO_2 mixing ratio. This could be due to the fact that the few trucks that did drive by passed directly under the measurement beam, whereas we were monitoring passive transport of ship plumes from the canal to the beam paths that was coincident with downwind mixing. There are distinct CO_2 peaks corresponding with our noting of trucks passing by the measurement site. Two trucks were observed passing by the experiment site at 12:09 and 12:11PM that resulted in one longer merged CO_2 peak. That is why the size of the CO_2 peak at around 12:10PM is larger than other peaks caused by truck emissions. In general, the baseline of CO_2 decreased as the day proceeded either due to increased photosynthesis during the day, or dilution of CO_2 sources in an expanding boundary layer as thermal convection increases. The number of trucks passing by the measurement site was higher than the number of ships. This

was not necessarily a drawback as we could also use truck plumes to demonstrate the methodology. We were left with two clear ship plumes. These two peaks belong to a Coast guard ship and the CSL Assiniboine, respectively. Linear regression and integration analysis were performed on the data from these two ship plumes along with a few other peaks associated with the truck emissions in order to determine the SO_2 emission factor and percentage of sulfur from ships and trucks.

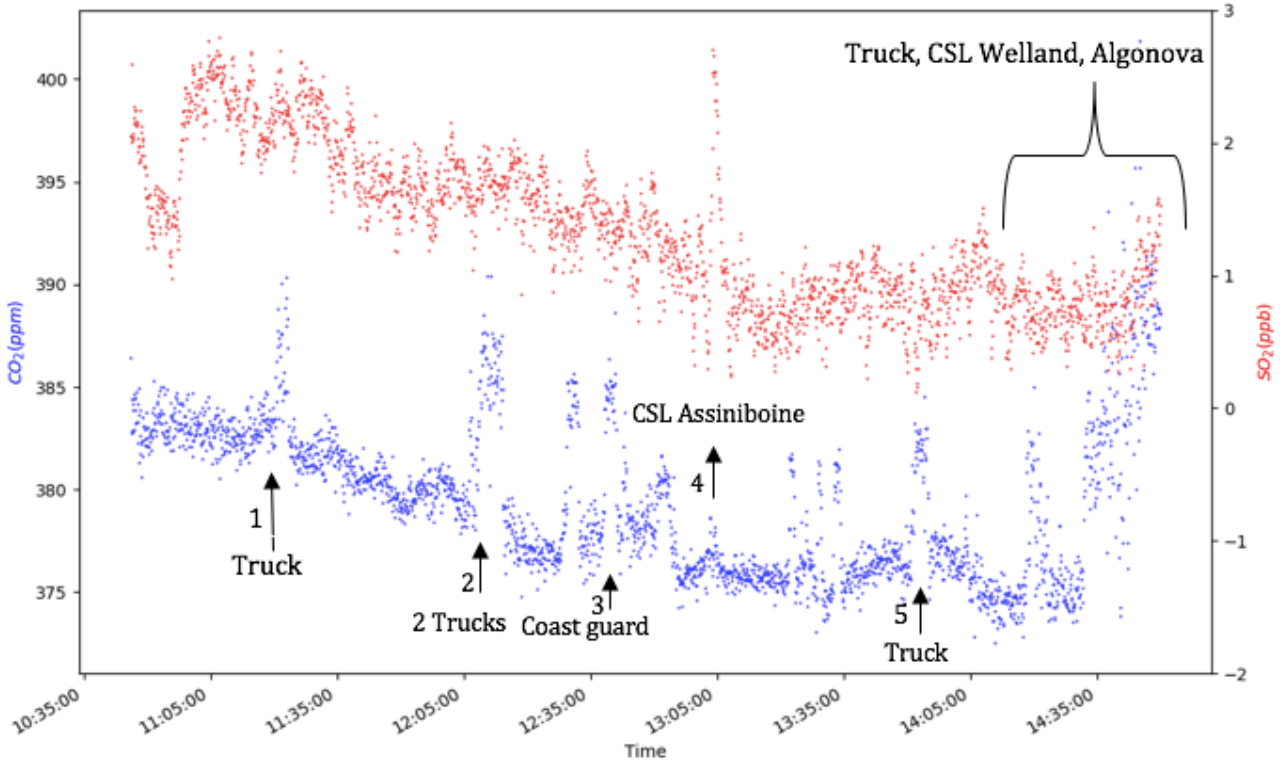

Figure 21: SO_2 and CO_2 mixing ratios versus time graph. Both CO_2 and SO_2 mixing ratios were stacked in to groups of 5 data points. Then, the EWMA technique was performed on each group of the data points in order to smooth the noise. SO_2 and CO_2 data points were averaged to 30 and 0.5 seconds respectively. The plume events for marine vessels and trucks are labelled on the graph.

3.2.1- Linear Regression Analysis for Aug 1, 2017 Results

In this section, 5 plume events associated with 5 different vessels on Aug 1, 2017 were identified in order to characterize the SO_2/CO_2 ratios from these sources. The SO_2/CO_2 ratios were identified

using two related methods as outlined in McLaren *et al*., 2012. The first method involves a linear least squares regression of the SO_2 to CO_2 using all the points within the plume event including suitable baseline points on each side of the plume. The plumes were chosen based upon the time of the CO_2 peaks, which were more obvious. The SO_2 peaks were less obvious or absent due to low sulfur content of the diesel fuel or marine fuels. The time intervals that were selected to represent each peak are summarized in Table 8. The time series graphs of SO_2 and CO_2 mixing ratios for each separate plume event are plotted in Figures 22 to 26. The linear regressions of SO_2 and CO_2 measurements for each of the 5 peaks are shown in Figures 27 to 31 in which the base-line has been subtracted. To subtract the baseline, the data from 20-30 seconds prior to and after each plume event were averaged and the average was considered as a base-line. Then, the average value was subtracted from each data point in the plume events. A trend line is shown for each correlation plot with a floating intercept. The equation of the line, the uncertainty of slope and R^2 values are mentioned in the figure captions (Figures 27 to 31).

Table 8: The time interval for each peak in order to graph the correlation plots.

Peak	Vessel	Time interval associated with the peak
1	Truck	11:20:00 – 11:23:30 AM
2	2 Trucks	12:07:30 – 12:14:30 PM
3	Coast Guard	12:37:20 – 12:41:10 PM
4	CSL Assiniboine	12:48:30 – 12:53:35 PM
5	Truck	13:50:00 – 13:56:05 PM

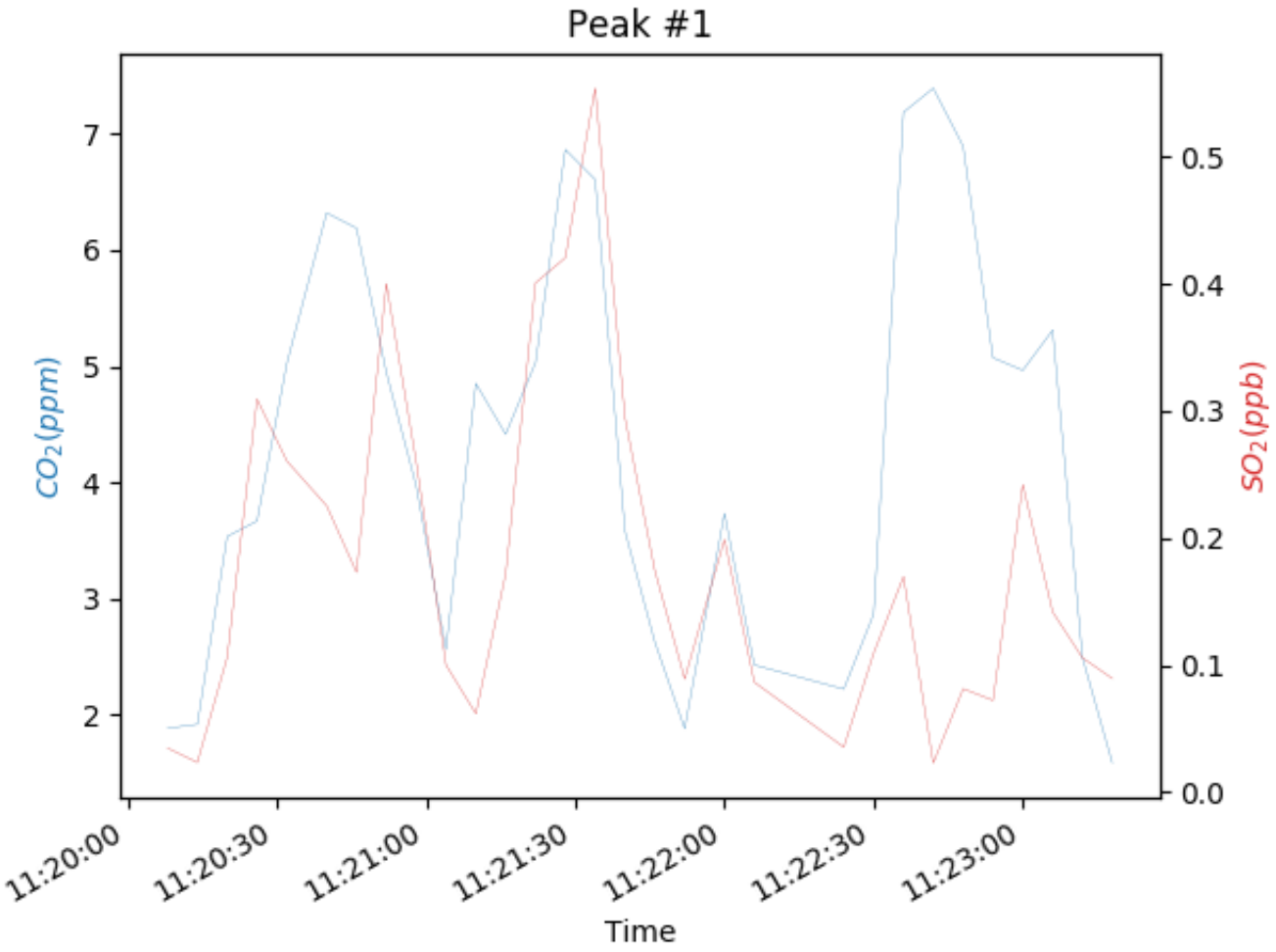

Figure 22: SO_2 and CO_2 mixing ratios versus time graph for the first peak that is associated with a plume truck observed within time interval of 11:19:30 – 11:23:30 AM.

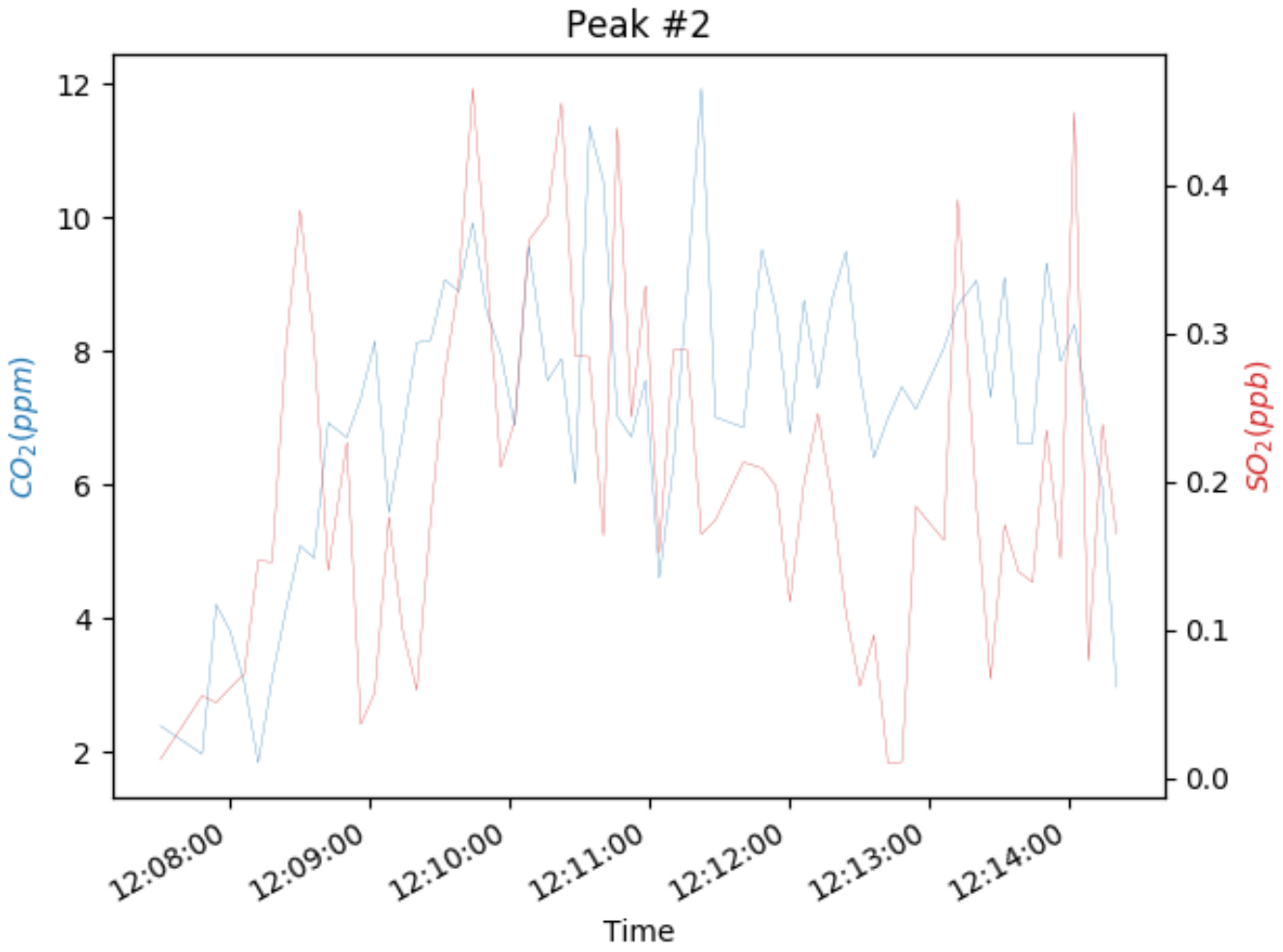

Figure 23: SO_2 and CO_2 mixing ratios versus time graph for the second peak that is associated with two trucks observed within time interval of 12:07:30 – 12:14:30 PM.

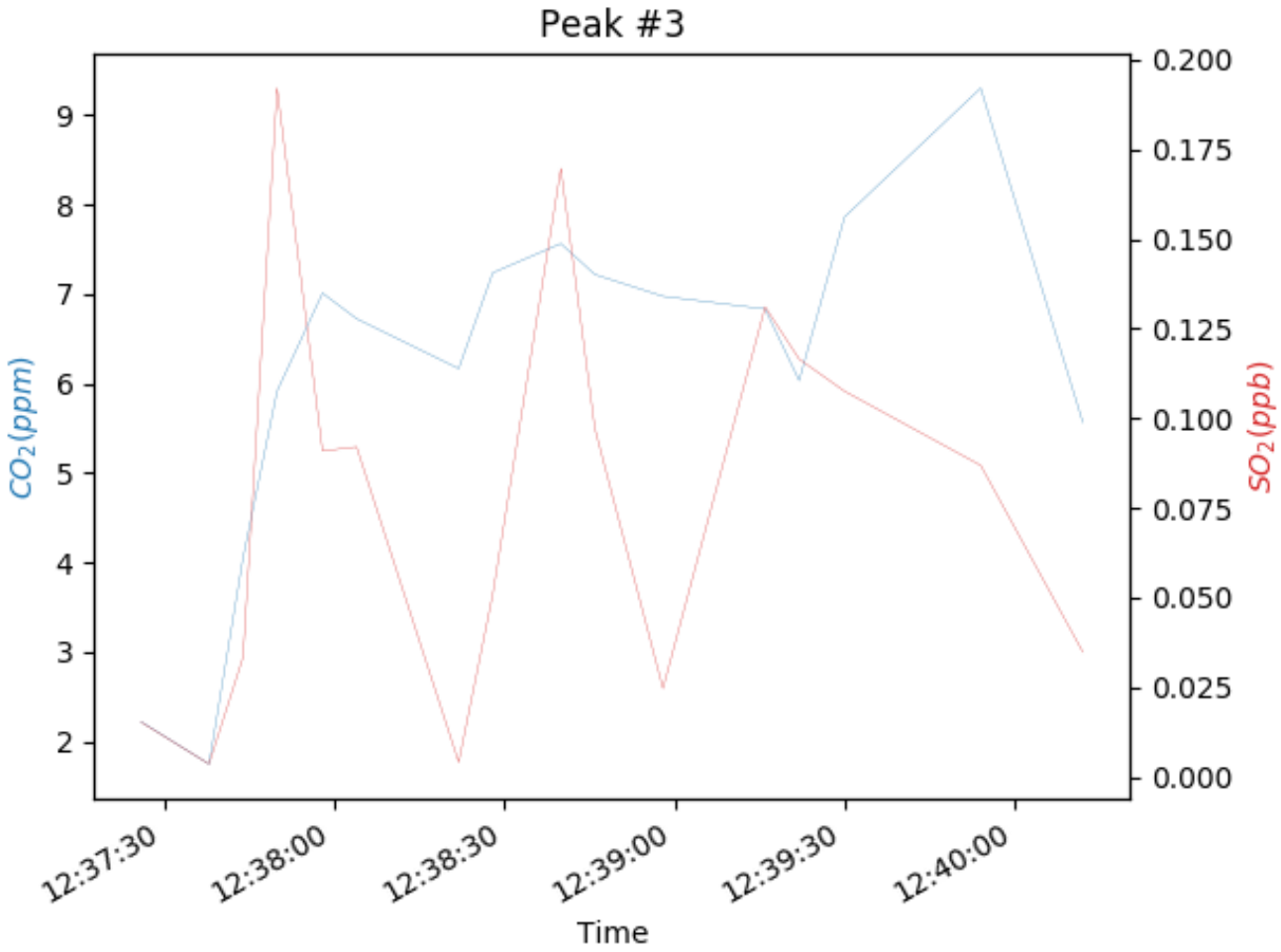

Figure 24: SO_2 and CO_2 mixing ratios versus time graph for the third peak that is associated with the coast guard observed within time interval of 12:37:17 – 12:41:10 PM.

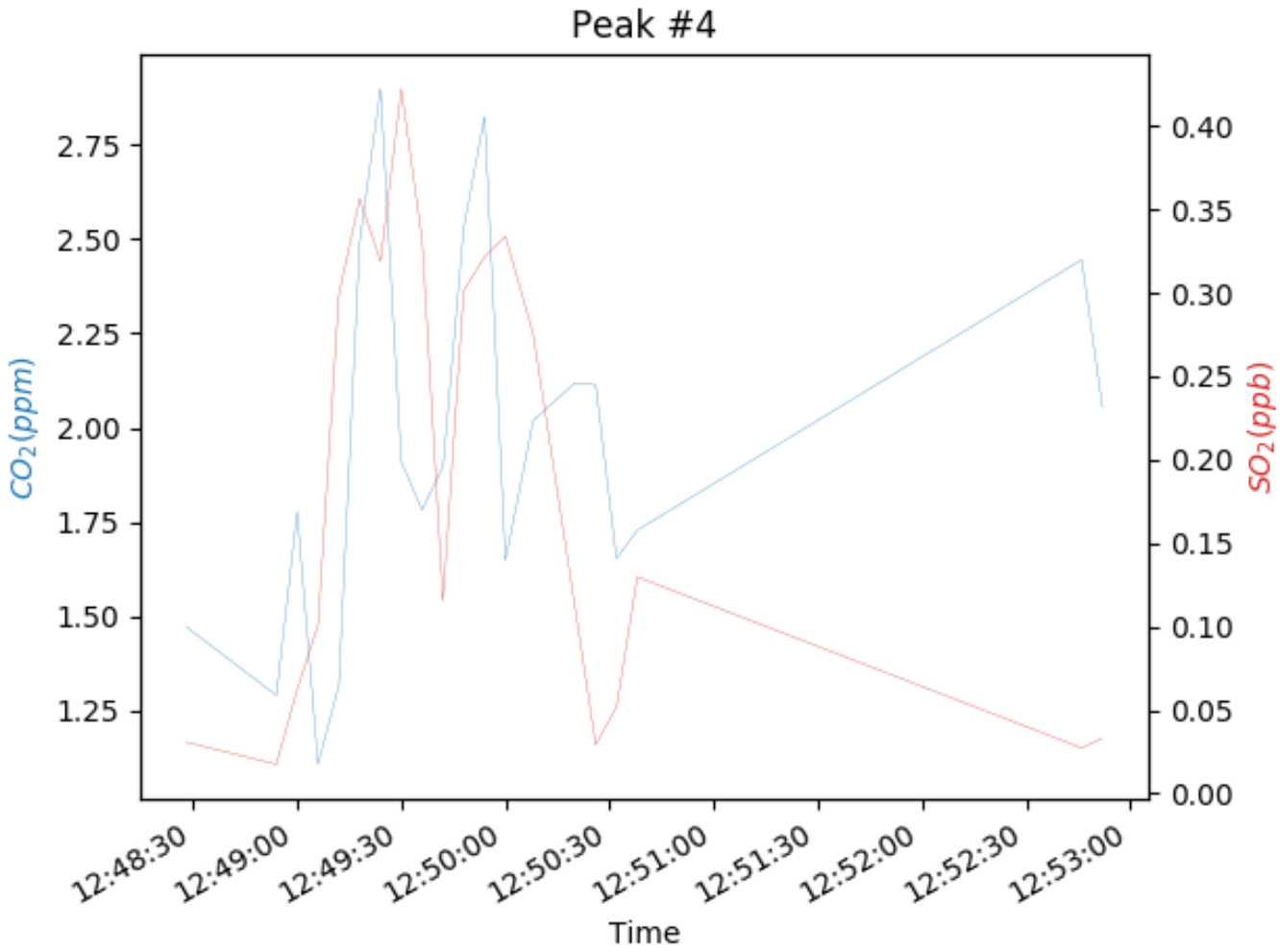

Figure 25: SO_2 and CO_2 mixing ratios versus time graph for the forth peak that is associated with the CSL Assiniboine observed within time interval of 12:48:30 – 12:53:35 PM.

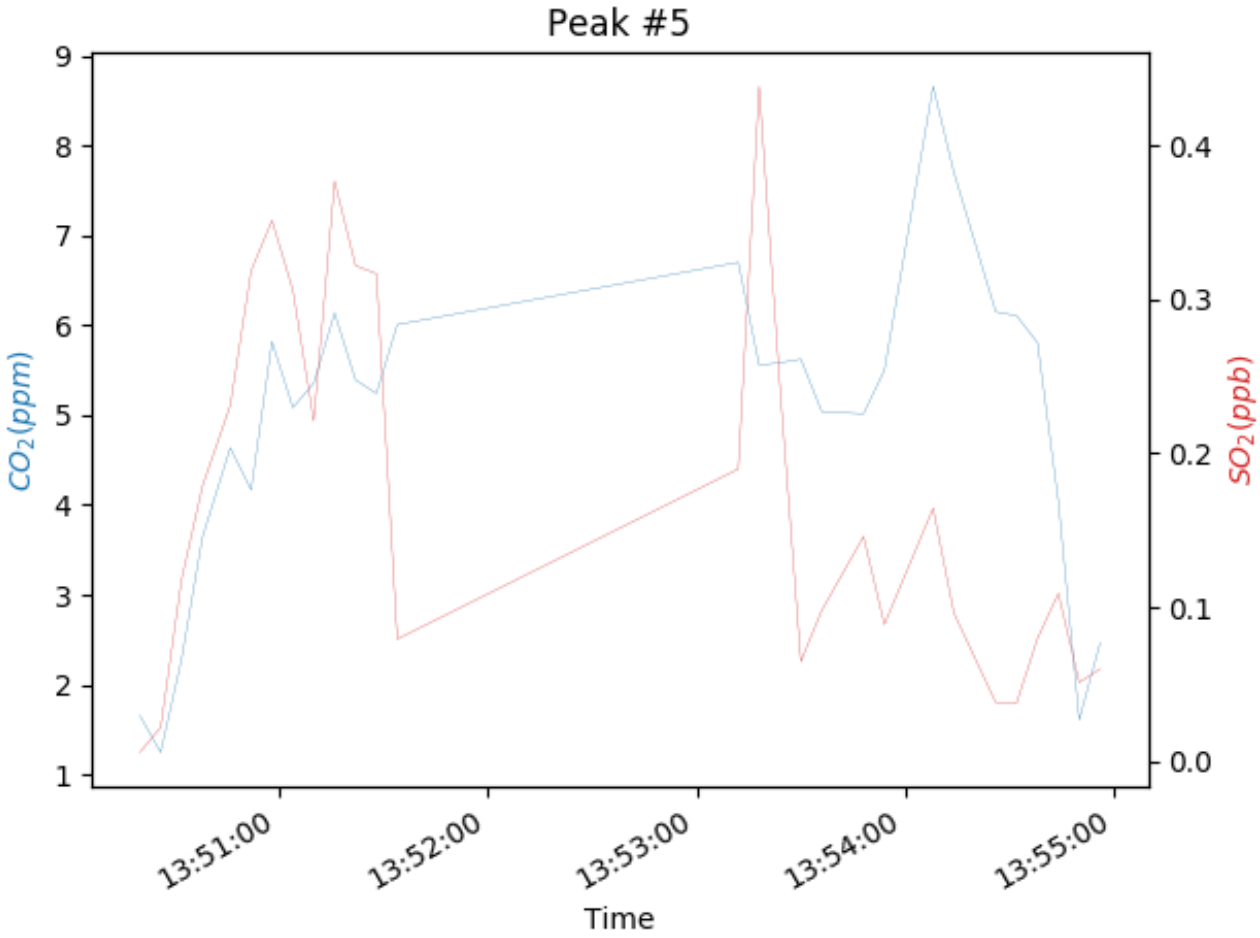

Figure 26: SO_2 and CO_2 mixing ratios versus time graph for the fifth peak that is associated with the truck observed within time interval of 13:50:00 – 13:56:05.

As can be seen in Figure 27, the slope along with its uncertainty of the correlation plot for the truck associated with peak 1 is 0.035 ± 0.004 (ppb/ppm) which represents $\Delta SO_2/\Delta CO_2$ ratio. The correlation plot for the two merged trucks plumes associated with peak 2 (Figure 28), indicates a slope of 0.015 ± 0.008 (ppb/ppm). Figures 29 and 30 show the correlation plots for the coast guard and CSL Assiniboine with slopes of 0.009 ± 0.006 and 0.088 ± 0.017 (ppb/ppm), respectively. The last correlation analysis is for the truck within the time interval of 13:50:00 – 13:56:05 (Figure 31) with a slope of 0.011 ± 0.009 (ppb/ppm). Looking at the 5 slopes, it is inferred that events 2 and 5 have similar slopes within their errors which are associated with trucks. Event 1 which is also

associated with a truck has a slightly higher slope than events 2 and 5. Event 3 (Coast guard) has the smallest slope. The highest slope belongs to peak 4 which is associated with the CSL Assiniboine which is a marine vessel.

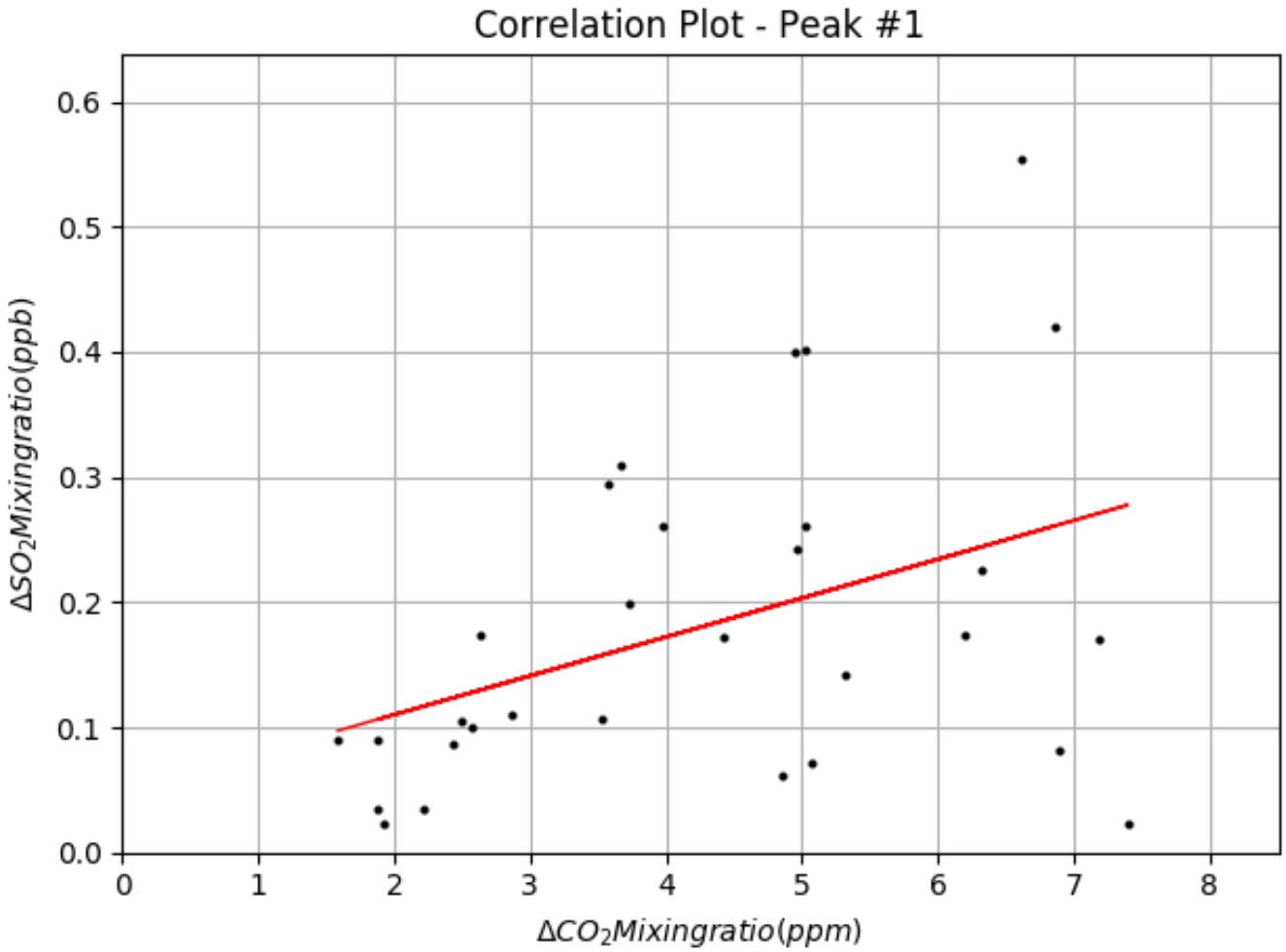

Figure 27: The linear regression of SO_2 and CO_2 measurements for the truck associated with peak 1. The equation of the correlation line for the truck is $SO_2 = (0.035 \pm 0.004) \times CO_2 + (0.068 \pm 0.020)$, $R^2 = 0.222$.

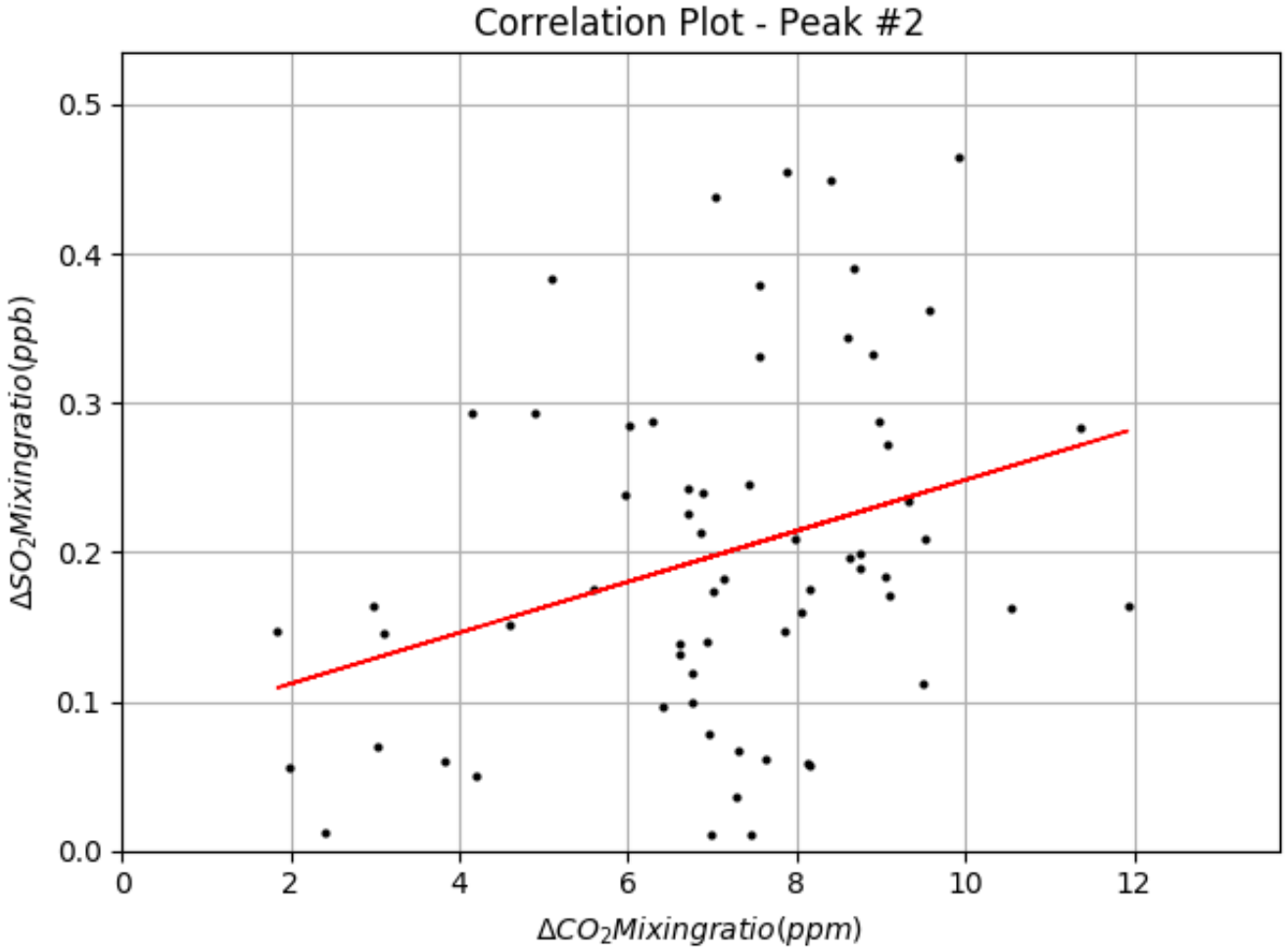

Figure 28: The linear regression of SO_2 and CO_2 measurements for the two trucks associated with peak 2. The equation of the correlation line is $SO_2 = (0.015 \pm 0.008)$ x $CO_2 + (0.120 \pm 0.049)$, $R^2 = 0.089$.

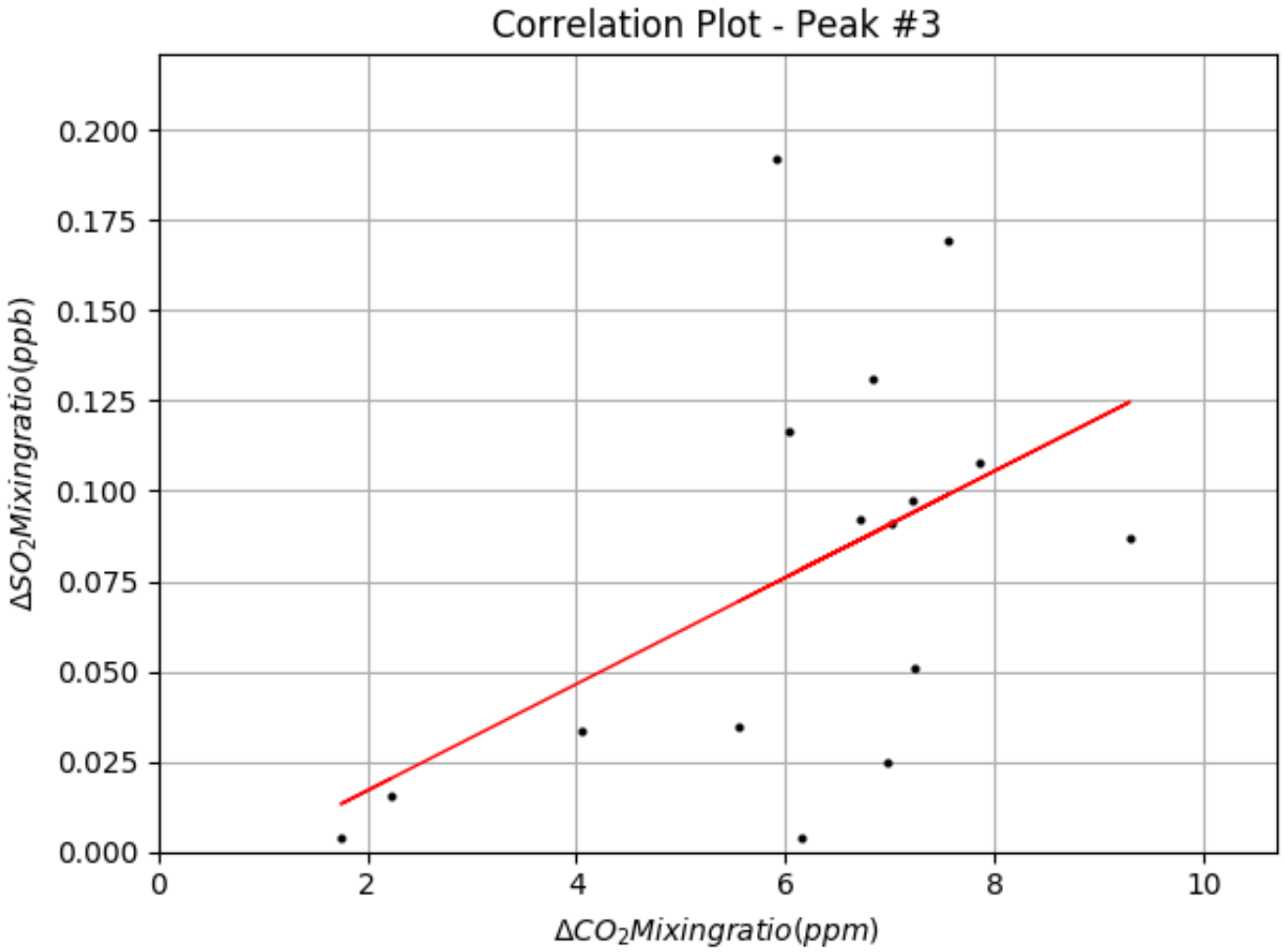

Figure 29: The linear regression of SO_2 and CO_2 measurements for the Coast guard. The equation of the correlation line is $SO_2 = (0.009 \pm 0.006)$ x $CO_2 + (0.032 \pm 0.052)$, $R^2 = 0.127$.

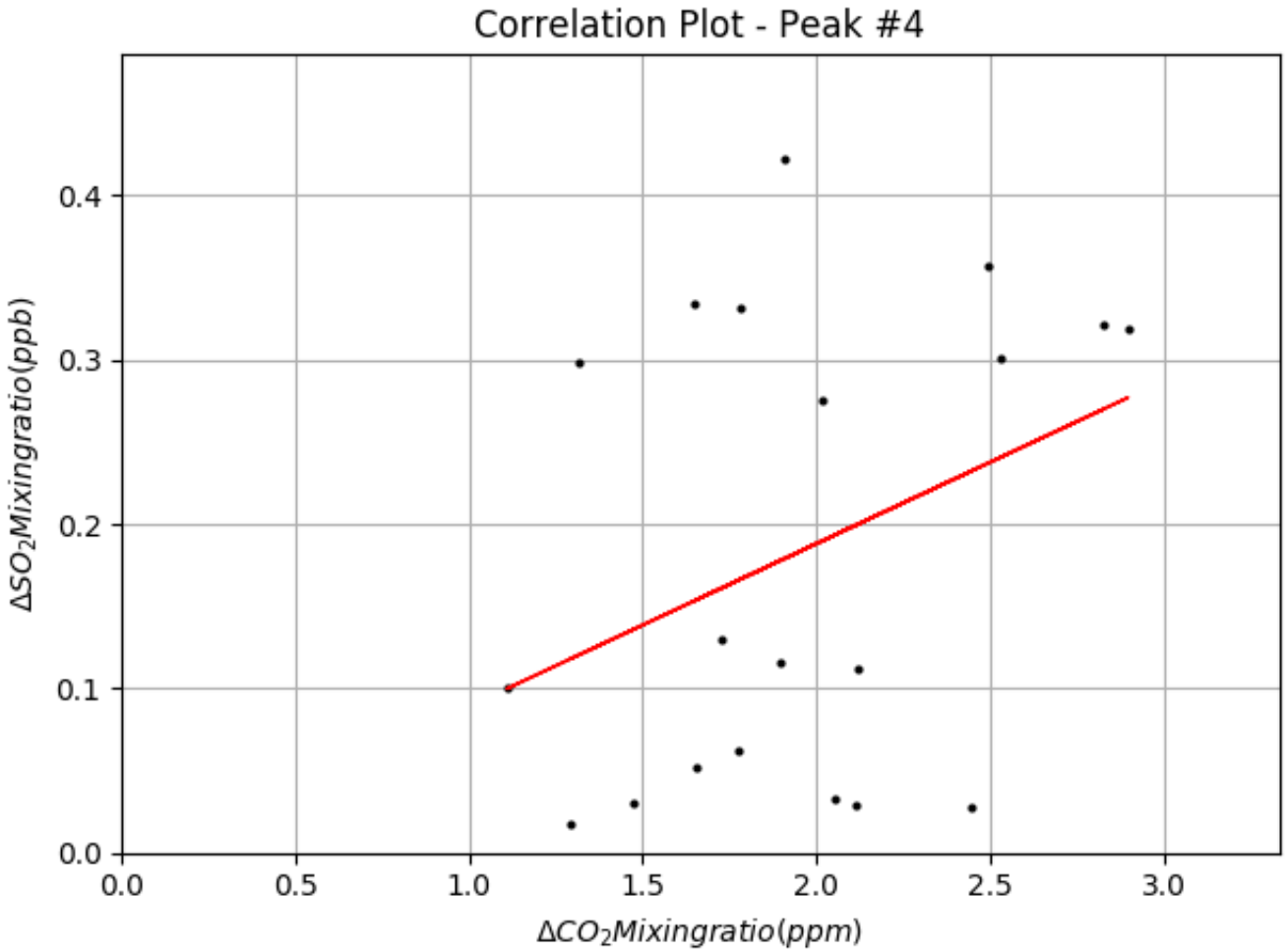

Figure 30: The linear regression of SO_2 and CO_2 measurements for CSL Assiniboine. The equation of the correlation line is $SO_2 = (0.088 \pm 0.017)$ x $CO_2 + (0.015 \pm 0.038)$, $R^2 = 0.097$.

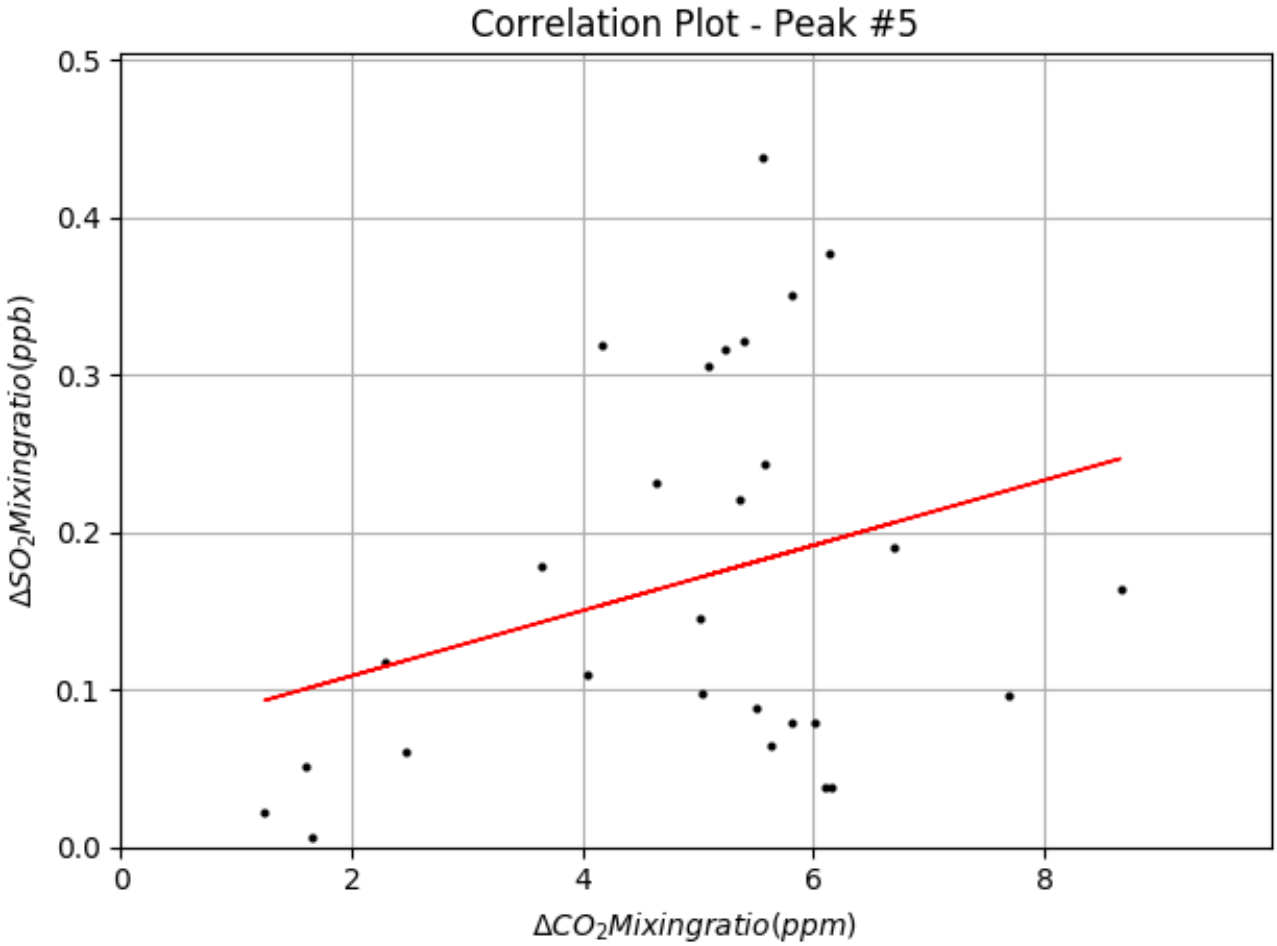

Figure 31: The linear regression of SO_2 and CO_2 measurements for a truck associated with peak 5. The equation of the correlation line is $SO_2 = (0.011 \pm 0.009)$ x $CO_2 + (0.143 \pm 0.065)$, $R^2 = 0.034$.

The slope of the correlation lines, which represents the $\Delta SO_2/\Delta CO_2$, was used to determine the emission factor (EF) and percentage of sulfur (%S) in the fuel for the five events and are summarized in Table 9. The emission factor and percentage of sulfur are calculated using equations 1 and 2 explained in the method section of this thesis (section 1.6). Looking at Table 9, the Coast guard and CSL Assiniboine ship plumes have emission factors of 0.043 ± 0.028 and 0.406 ± 0.078 (g_{SO2}/kg_{fuel}). The SO_2 emission factor of CSL Assiniboine is 10 times more than the emission factor of Coast guard. CSL Assiniboine, has the highest EF(SO_2) amongst all. Looking at the Trucks' emission factors, it is inferred that all the trucks' events have similar emission factors

within their errors. Overall, the percentage of sulfur and emission factors of SO_2 for all the plume events are significantly low which is interpreted as the direct result of strict sulfur emissions on road and in sulfur emission control areas (SECA) enforcement which requires marine vessels to burn low sulfur fuels. The detection limits for the percentage of sulfur and SO_2 emission factor are also summarized in Table 9. The average detection limit for the percentage of sulfur in fuel and EF(SO_2) are 0.006% and 0.120 (g $_{SO2}$/ kg $_{fuel}$), respectively. In this study, only three plumes had SO_2 emissions that were statistically different from zero and above detection limit, peak 1 (truck), peak 4 (CSL Assiniboine ship) and peak 5 (truck).

Table 9: The calculated emission factor and percentage of sulfur in fuel along with their detection limits for the five plume events.

Peak	Vessel	Slope, SO_2/CO_2 (ppb/ppm)	Emission Factor, (g $_{SO2}$/ kg $_{fuel}$)	Percentage of sulfur (%)	Detection limit (3σ) of Emission Factor (g $_{SO2}$/ kg $_{fuel}$)	Detection limit (3σ) of % S
1	Truck	0.035 ± 0.004	0.161 ± 0.019	0. 008± 0.001	0.057	0.003
2	2 Trucks	0.015 ± 0.008	0.067 ± 0.036	0.003 ± 0.002	0.107	0.005
3	Coast Guard	0.009 ± 0.006	0.043 ± 0.028	0.002 ± 0.001	0.083	0.004
4	CSL Assiniboine	0.088 ± 0.017	0.406 ± 0.078	0.020 ± 0.004	0.233	0.012
5	Truck	0.011 ± 0.009	0.049 ± 0.041	0.002 ± 0.002	0.123	0.006

3.2.2- Integration Analysis of The Peaks

In the second method, the $\Delta SO_2/\Delta CO_2$ ratio is calculated via the integrated excess pollutant during the plume event, with suitable background subtraction. A baseline is manually determined for each event. To subtract the baseline, the data from 20-30 seconds prior to and after each plume event were averaged and the average was considered as a base-line. Then, the average value was

subtracted from each data points in the plume events. Composite trapezoidal rule was used for integrating the area under the graph. The results are summarized in Table 10.

$$\frac{SO2}{CO2} = \frac{\int \Delta SO2 \, dt}{\int \Delta CO2 \, dt} \qquad \text{Equation 13}$$

Table 10: The calculated area under the SO_2 and CO_2 curves and their corresponding SO_2/CO_2 ratio values using python programming.

Peak	Vessel	Area under SO_2 curve (ppb-sec)	Area under CO_2 curve (ppm-sec)	$\Delta SO_2/\Delta CO_2$ (ppb-sec/ppm-sec)
1	Truck	43.68 ± 8.90	851.65 ± 61.05	0.051 ± 0.008
2	2 Trucks	87.71 ± 38.48	2821.71 ± 83.33	0.031 ± 0.013
3	Coast Guard	16.50 ± 6.27	1217.18 ± 242.65	0.013 ± 0.002
4	CSL Assiniboine	33.46 ± 0.36	506.19 ± 26.21	0.066 ± 0.003
5	Truck	49.49 ± 5.55	1553.45 ± 16.27	0.032 ± 0.003

The $\Delta SO_2/\Delta CO_2$ ratios obtained from integration analysis were used to determine the emission factor (EF) and percentage of sulfur for the five events and are summarized in Table 11. The SO_2 emission factor for peak 4 is the highest just as the linear regression method. Also, the trucks are having similar EF(SO_2) within their errors. The percentage of sulfur for all the plume events are much lower than the 0.1% which is the SECA limit. The detection limits for the percentage of sulfur and SO_2 emission factor are also summarized in Table 9. The average detection limit for the percentage of sulfur and EF(SO_2) are 0.004% and 0.083 (g_{SO2}/ kg_{fuel}), respectively.

Table 11: The calculated emission factor and percentage of sulfur along with their detection limits for the five plume events using the integration analysis.

Peak	Vessel	$\Delta SO_2/\Delta CO_2$ (ppb-sec/ppm-sec)	Emission Factor (g_{SO2}/ kg_{fuel})	Percentage of sulfur (%)	Detection limit (3σ) of Emission Factor (g_{SO2}/ kg_{fuel})	Detection limit (3σ) of % S
1	Truck	0.051 ± 0.008	0.237 ± 0.037	0.012 ± 0.002	0.111	0.006
2	2 Trucks	0.031 ± 0.013	0.144 ± 0.061	0.007 ± 0.003	0.184	0.009
3	Coast Guard	0.013 ± 0.002	0.062 ± 0.011	0.003 ± 0.001	0.032	0.002
4	CSL Assiniboine	0.066 ± 0.003	0.307 ± 0.013	0.015 ± 0.001	0.039	0.002
5	Truck	0.032 ± 0.003	0.148 ± 0.016	0.007 ± 0.001	0.047	0.002

Tables 10 and 11 are summarized in Table 12. It is inferred that the two methods: linear regression analysis and integration analysis use the same concept for calculating $\Delta SO_2/\Delta CO_2$ ratio for each plume event. As expected, they generate similar results within error. Peak 4 that is CSL Assiniboine ship plume has the highest SO_2 emission factor and percentage of sulfur for both methods. The values obtained from both methods are relatively close to each other for each plume event. For example, looking at the SO_2 emission factor values calculated for peak 4 associated with CSL Assiniboine, the EF(SO_2) values calculated by linear regression and integration analysis are 0.406 ± 0.078 and 0.307 ± 0.013 (g_{SO2}/ kg_{fuel}), respectively. In general, the percentage of sulfur and SO_2 emission factors are significantly low. The relatively low SO_2 emission factors in marine vessel observations are likely the direct result of strict sulfur emission control areas (SECA) regulations. Beginning in 2015, fuel used by vessels operating in sulfur emission control areas cannot exceed 0.1% sulfur and looking at Table 12, the sulfur fuel contents for all the vessels are much lower than 0.1%.

Table 12: The calculated emission factor and percentage of sulfur for Linear regression analysis and Integration analysis.

		Linear Regression Analysis		Integration Analysis	
Peak	**Vessel**	**Emission Factor (g_{SO2}/ kg $_{fuel}$)**	**Percentage of sulfur (%)**	**Emission Factor (g_{SO2}/ kg $_{fuel}$)**	**Percentage of sulfur (%)**
1	Truck	0.161 ± 0.019	0. 008± 0.001	0.237 ± 0.037	0.012 ± 0.002
2	2 Trucks	0.067 ± 0.036	0.003 ± 0.002	0.144 ± 0.061	0.007 ± 0.003
3	Coast Guard	0.043 ± 0.028	0.002 ± 0.001	0.062 ± 0.011	0.003 ± 0.001
4	CSL Assiniboine	0.406 ± 0.078	0.020 ± 0.004	0.307 ± 0.013	0.015 ± 0.001
5	Truck	0.049 ± 0.041	0.002 ± 0.002	0.148 ± 0.016	0.007 ± 0.001

4- Conclusions and future work:

This study showed that the fuel-based emission factor of SO_2 in plumes can be measured through simultaneous measurement of the SO_2 pollutant and CO_2 within the same path length of air. In this study, an absorption path was established close to a well-frequented waterway of Welland canal, Ontario utilizing light sources from active-DOAS and TDLAS along with retro-reflectors. Active-DOAS and TDLAS were side by side with close proximity and the ship plumes were passively transported to the instruments through a judicious choice of placement of the instrument on the east side of the canal. Continuous measurements of SO_2 and CO_2 mixing ratios were performed as ships passed through the Welland Canal. A linear regression and integration analysis method were used and compared to determine a mass-based emission factor and sulfur content. Finally, the amount of sulfur in the fuel was calculated to verify compliance. The two methods had similar results within their errors. The calculated SO_2 emission factors were relatively low due to low sulfur

content in the fuels. Our measurements confirmed that the monitored marine vessels trafficking in Welland Canal were not significant sources of sulfur. The marine vessels CSL Assiniboine and the coast guard had the SO_2 emission factors of 0.406 ± 0.078 and 0.043 ± 0.028 (g_{SO2}/ kg_{fuel}), respectively using linear regression analysis. The sulfur fuel content for all the monitored vessels were much lower than 0.1% and this could be the direct result of strict sulfur emission control area (SECA) enforcement.

There are several factors influencing the accuracy of the calculated values of SO_2 emission factor and sulfur content for each ship. The sulfur fuel percentage formula assumes a 100% conversion from sulfur to SO_2 during combustion, which is only true for an idealized combustion process. Earlier studies have showed that not all the sulfur in the fuel is emitted as SO_2. Experiments have showed that 1 to 19% of the sulfur in the fuel is emitted in other forms, possibly SO_3 or H_2SO_4 (Moldanova *et al*., 2009). Therefore, the assumption that all sulfur is emitted as SO_2 yields an underestimation of the true sulfur content in the fuel. Also, chemical losses of SO_2 and CO_2 in the plume during the transit time is assumed to be small. Because of the proximity of the ships to the measurement site, the ship plumes were fresh and conversion of SO_2 to sulphate would be negligible. It is important to note that apart from emission factors, activity factors and fuel consumption information are important for analyzing the magnitude of marine vessel sources.

The number of marine vessels trafficking in Welland canal was not as high as expected. Inevitably, data analysis was performed on a few marine plumes. On August 1, 2017, only 4 marine vessels were monitored and from these 4 vessels, only 2 of them caused a significant increase in SO_2 level. Our method was straightforward in terms of association of a ship with a plume. The combination of trace gases peak time, the wind direction, and the ship arrival time enabled the identification of the peak related to a specific ship. However, only the events that had noticeable CO_2 or SO_2 peaks were analyzed.

This research developed and demonstrated a new method that could be used to monitor emissions from ships in areas where a beam can transect ship plumes. This will ensure compliance to IMO regulations on controlling sulfur content in fuel. The long path DOAS (LP-DOAS) is a promising technique for monitoring the ship emissions since it is capable of simultaneously measuring trace gases. However, this technique requires a proper measurement area to provide an ideal measurement path. The selected measurement site was not ideal to perform this experiment as it was impacted by truck emissions in addition to ship emissions. However, this project was only a demonstration of the feasibility of the technique monitoring the percentage of sulfur in ship fuels. The other limitation of this method is the wind direction as this technique requires a suitable wind direction to carry the plumes to the beams. Therefore, the experimental site needs to be situated within the direction of the prevailing wind. To add more, strong wind is not suitable since it facilitates the plume dilution. For future experiments, an ideal location for this methodology would be to have the beam directly transect the ship plumes instead of depending on the passive transport of the plumes to the beam path. An example of such a location would be to have the beam transect the waterway at an elevated height (higher than the highest anticipated stack height would exist ~ 30-40 m), such as under the Lions Gate Bridge in Vancouver or a similar site on the east coast of Canada in Halifax port. Also, in terms of alternative instruments, MAX-DOAS could be used since it would allow monitoring the plumes at a given altitude range without need for a "mechanical construction" of a given height.

5- Bibliography:

Alicke, B., Hebestreit, K., Stutz, J., Platt, U. (1999). Iodine oxide in the marine boundary layer, Nature, 397, 572–573.

Beecken, J., Mellqvist, J., Salo, K., Ekholm, J., Jalkanen. J.P. (2014). Airborne emission measurements of SO_2, NO_X and particles from individual ships using a sniffer technique, Atmos. Chem. Phys, 7(7): 1957-1968.

Berg, N., Mellqvist, J., Beecken, J., Johansson, J. (2010). Ship Emission Measurements by the Chalmers IGPS System during the Rotterdam campaign 2009 (Report No.5). Göteborg, Sweden: Department of Radio and Space Science Chalmers University of Technology.

Berglen, T.F., Bernsten, T.K., Isaksen, I.S.A., Sundet, J.K. (2004). A global model of the coupled sulfur/oxidant chemistry in the troposphere: the sulfur cycle, J. Geophys. Res, 109, D19310.

Bogumil, K., Orphal, J., Homann, T., Voigt, S., Spietz, P., Fleischmann, O.C., Vogel, A., Hartmann, M., Bovensmann, H., Frerick, J., Burrows, J.P. (2003). Measurements of molecular absorption spectra with the SCIAMACHY pre-flight model: Instrument characterization and reference data for atmospheric remote sensing in the 230-2380 nm region, J. Photochem. Photobiol, 157, 167-184.

Brasseur, G.P., Orlando, J.J., Tyndall, G.S.: Chapter no. 5: Trace gas exchanges and biogeochemical sulfur cycles, Oxford University Press, Inc., 1999.

Burgard, D.A., Bria, C.R.M. (2016). Bridge-based sensing of NO_X and SO_2 emissions from ocean-going ships, Atmospheric Environment, 136, 54-60.

Cappa, C.D., Williams, E.J., Lack, D.A., Buffaloe,G.M., Coffman, D., Hayden, K.L., Lerner, B.M., Li, S.M., Massoli, P., McLaren, R., Nuaanman, I., Onasch, T.B., and Quinn, P.K. (2014). A Case Study into the Measurement of Ship Emissions from Plume Intercepts of the NOAA Ship Miller Freeman, Atmos. Chem. Phys, 14, 1337-1352.

Corbett, J.J., Fischbeck, P.S. (2000). Emissions from Waterborne Commerce in United States Continental and Inland Waters, Environ. Sci. Technol, 34 (15), 3254–3260.

Corbett, J.J., Winebrake, J.J., Green, E.H., Kasibhatla, p., Eyring, V., Lauer, A. (2007). Mortality from Ship Emissions: A Global Assessment, Environ. Sci. Technol, 41, 8512–8518.

Endresen, O., Bakke, J., Sorgard, E., Berglen, T.F., Holmvang, P. (2005). Improved modeling of ship SO_2 emissions -a fuel-based approach, Atmos. Environ, 39(20): 3621-3628

EPA. 2008. International Maritime Organization Adopts Program to Control Air Emissions from Oceangoing Vessels. (Program Announcement No. EPA420-F-08- 033). U.S. EPA.

European Commission, Entec UK Limited. (2002). Quantification of emissions from ships associated with ship movements between ports in the European Community.

Eyring, V., Kohler, H.W., Van, J.A., Lauer, A. (2005). Emissions from international shipping: 1. The last 50 years, J. Geophys. Res. 110 (D17305): 1-12.

Flagan, R.C., Seinfeld, J.H. (1988). Fundamentals of Air Pollution Engineering. Prentice-Hall, Englewood Cliffs, NJ, 168-185.

Harris, G.W., Mackay, G. I., Iguchi, I., Mayne, L.K., Schiff, H.I. (1989). Measurements of formaldehyde in the troposphere by tunable diode laser absorption spectroscopy, J. Atmos. Chem, 3, 119–137.

Harris, G.W., Klemp, D., Zenker, T., Burrows, J.P., Mathieu, B. (1992). Tunable diode laser measurements of trace gases during the 1988 Polarstern cruise and intercomparisons with other methods, J. Atmos. Chem, 15, 315–326.

Honninger, G., Von Friedeburg, C., Platt, U. (2004). Multi axis differential optical absorption spectroscopy (MAX-DOAS), Atmos. Chem. Phys, 4, 231-254.

IMO, 2015. Third IMO GHG Study 2014 [WWW Document]. Third IMO GHG Study 2014.

International Council on Clean Transportation. (2007). Air pollution and greenhouse gas emissions from ocean-going ships: Impacts, mitigation options and opportunities for managing growth, executive summary, 15 pp., ICCT Publ., Washington, D. C.

Jonson, J., Tarrason, L., Bartnicki, J. (2000). Effects of international shipping on European pollution levels. Oslo, Norway: EMEP/MSC-W Note 5.

Kattner, N., Mathieu-Uffing, B., Burrows, J.P., Ritchter, A., Schmolke, S., Seyler, A., Wittrock, F. (2015). Monitioring compliance with sulfur content regulations of shipping fuel by in situ measurements of ship emissions, Atmos. Chem. Phys, 15, 10087-10092.

Kraus, S. (2006). DOASIS: A Framework Design for DOAS, Ph.D. thesis, University of Mannheim.

Lack, D. A., et al. (2009). Particulate emissions from commercial shipping: Chemical, physical, and optical properties, J. Geophys. Res, 114, D00F04.

Lack, D.A., Cappa, C.D., Langridge, J., Bahreni,R., Buffaloe, G., Brock, C., Cerully, K., Coffman, K., Hayden, K.L., Holloway, J., Lerner, B., Massoli, P., Li, S.M., McLaren, R. Middlebrook, A.M., Moore, R., Nenes,A., Nuaaman, I., Onasch, T.B., Peischl, J., Perring,A., Quinn, P.K., Ryerson, T., Schwartz, J.P., Spackman, R., Wofsy, S.C., Worsnop, D., Xiang, B., Williams, E. (2011). Impact of Fuel Quality Regulation and Speed Reductions on Shipping Emissions: Implications for Climate and Air Quality, Environ. Sci. Techn, 45 (20): 9052-9060.

Levenberg, K. (1944). A method for the solution of certain non-linear problems in least squares, Quarterly of Applied Mathematics, 2, 164–168.

Lohmann, U., Feichter, J. (2005). Global indirect aerosol effects: A review, Atmos. Chem. Phys, 5, 715–737.

Mackay, G.I., Karecki, D.R., Schiff, H. I. (1996). Tunable diode laser absorption measurements of H_2O_2 and HCHO during the Mauna Loa Observatory Photochemistry Experiment, J. Geophys. Res, 101(14): 721–14,728.

Matthias, V., Bewersdorff, I., Aulinger, A., Quante, M. (2010). The contribution of ship emissions to air pollution in the North Sea regions, Environ. Pollut, 158, 2241–2250.

McLaren, R., Wojtal, P., Halla, J.D. Mihele, C., Brook, J. (2012). A survey of NO_2:SO_2 emission ratios measured in marine vessel plumes in the Strait of Georgia, Atmos. Environ, 46, 655-658.

Moldanova, J., Fridell, E., Popovicheva, O., Demirdjian, B., Tishkova, V., Faccinetto, A., Focsa, C. (2009). Characterization of particulate matter and gaseous emissions from a large ship diesel engine, Atmos. Environ, 43, 2632–2641.

Perner, D., Ehhalt, D., Paetz, H., Platt, U., Roeth, E., Volz, A. (1976). OH-Radicals in the lower troposphere, Geophysical Research Letters, 3, 466–468.

Plane, J. and Smith, N. (1995). Atmospheric monitoring by differential optical absorption spectroscopy, Advances in Spectroscopy, 24, 223–223.

Platt, U., Perner, D., Petz, H. (1979). Simultaneous measurement of atmospheric CH_2O, O_3, and NO_3 by differential optical absorption, Journal of Geophysical Research: Oceans, 84, 6329–6335.

Platt, U., Perner, D., Harris, G., Winer, A., Pitts, J. (1980). Observations of nitrous acid in an urban atmosphere by differential optical absorption, Nature, 285, 312–314.

Platt, U. and Stutz, J. (2008). Differential optical absorption spectroscopy, Springer.

Sanders, R., Solomon, S., Carroll, M.A., Schmeltekopf, A.L. (1989). Visible and near- ultraviolet spectroscopy at McMurdo Station, Antarctica, 4. overview and daily measurements of NO_2, O_3 and OClO in 1989, J. Geophys. Res, 94, 11381, 1989.

Schiff, H.I., Hastie, D.R., Mackay, G.I., Iguchi, T., Ridley, B.A. (1983). Tunable diode laser systems for measuring trace gases in tropospheric air, Environ. Sci. Technol, 17, 352–364.

Schiller, C.L., Locquiao, S., Johanson, T.J., Harris, G.W. (2001). Atmospheric measurements of HONO by Tunable Diode Laser Absorption Spectroscopy, Journal of Atmospheric Chemistry, 40, 275-293.

Schreier, S.F., Peters, E., Richter, A., Lampel, J., Wittrock, F., Burrows. J.P. (2015). Ship-based MAX-DOAS measurements of tropospheric NO_2 and SO_2 in the South China and Sulu Sea, Atmospheric Environment, 102, 331-343.

Skoog, D.A., Holler J., Nieman, T.A. (1998). Principle of instrumental analysis. 5th ed. Philadelphia. Saunders College Pub.

Stockwell, W., Calvert, J. (1983). The Mechanism of the HO-SO2 Reaction, Atmos. Environ,17, 2231–

2235.

Textor, C., Graf, H.F., Timmreck, C., Robock, A. Emissions of Atmospheric Trace Compounds, chap. Emissions from volcanoes, pp. 269–303, Klewer, Dordrecht, Netherlands, 2004.

Tuttle, K. (1995). Combustion-generated emissions in marine propulsion systems. Proceedings of Ship Design and Operation in Harmony with the Environment. (ss. 311-232). Jersey City, NJ: Society of Naval Architects and Marine Engineers.

UNCTAD RMT, United Nations Conference on Trade and Development, Review of Maritime Transport, 2014.

European Commission, Entec UK Limited. (2002). Quantification of emissions from ships associated with ship movements between ports in the European Community.

U.S. EPA. 1994. Supplement to the second addendum (1986) to air quality criteria for particulate matter and sulfur oxides (1982): Assessment of new findings on sulfur dioxide and acute exposure health effects in asthmatic individuals. EPA/600/FP-93/002. Washington, DC. http://cfpub.epa.gov/ncea/cfm/recordisplay.cfm?deid=96580

Volkamer, R., Molina, L.T., Molina, M.J., Shirley, T., Brune, W.H. (2005). DOAS measurement of glyoxal as an indicator for fast VOC chemistry in urban air, Geophysical Research Letters, 32(8): 1-4.

Werle P.W. (2004). Diode-Laser Sensors for In-Situ Gas Analysis. Laser in Environmental and Life Sciences. Springer, Berlin, Heidelberg.

Williams, E.J., Lerrier, B.M., Murphy, P.C., Herndon, S.C., Zahniser, M.S. (2009). Emissions of NO_X, SO_2, CO, and HCHO from commercial marine shipping during Texas Air Quality Study (TexAQS) 2006, J. Geophys. Res. Atmos, 114, D21306.